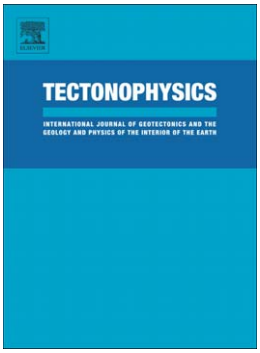

Synkinematic skarns and fluid drainage along detachments: The West Cycladic Detachment System on Serifos Island (Cyclades, Greece) and its related mineralization

M. Ducoux, Y. Branquet, L. Jolivet, L. Arbaret, B. Grasemann, A. Rabillard, C. Gumiaux, S. Drufin

PII: S0040-1951(16)30602-3
DOI: doi:10.1016/j.tecto.2016.12.008
Reference: TECTO 127351

To appear in: *Tectonophysics*

Received date: 23 February 2016
Revised date: 30 November 2016
Accepted date: 5 December 2016

Please cite this article as: Ducoux, M., Branquet, Y., Jolivet, L., Arbaret, L., Grasemann, B., Rabillard, A., Gumiaux, C., Drufin, S., Synkinematic skarns and fluid drainage along detachments: The West Cycladic Detachment System on Serifos Island (Cyclades, Greece) and its related mineralization, *Tectonophysics* (2016), doi:10.1016/j.tecto.2016.12.008

Synkinematic skarns and fluid drainage along detachments: the West Cycladic Detachment System on Serifos Island (Cyclades, Greece) and its related mineralization

M. Ducoux[1,2,3], Y. Branquet[1,2,3,4], L. Jolivet[1,2,3], L. Arbaret[1,2,3], B, Grasemann[5], A. Rabillard[1,2,3], C. Gumiaux[1,2,3], S. Drufin[1,2,3]

[1] Université d'Orléans, ISTO, UMR 7327, 45071 Orléans, France

[2] BRGM, ISTO, UMR 7327, BP 36009, 45060 Orléans, France

[3] CNRS/INSU, UMR 7327, 45071 Orléans, France

[4] Géosciences Rennes, UMR CNRS 6118, OSUR, Université de Rennes 1, 35042 Rennes, France

[5] Department for Geodynamics and Sedimentology, University of Vienna, Althanstrasse 14, 1090 Vienna, Austria

Abstract

Back-arc extension in the Aegean Sea has been accommodated by several large-scale detachments such as the West (WCDS) and the North Cycladic Detachment System in the Oligocene and Miocene. On Serifos Island the SE strand of the WCDS is exposed, which is syn-kinematically intruded by a granodioritic pluton. As skarns represent metasomatic reactions near the contact between intrusions and the host rocks, they sign the position of the main drains used by fluids. While the mineralogy of the Serifos skarns is well known, geometrical and kinematic relations between the detachments and ore bodies remain poorly studied. This study allows us distinguishing different types of skarn, high-temperature skarns as (1) massive garnet endoskarns, (2) ribbon and "bubble" garnet-pyroxene endoskarns, (3) garnet-pyroxene cracks exoskarns, and medium-temperature skarns as (4) pyroxene +/-

ilvaite-bearing skarn breccias within the Meghàlo Livadhi and Kàvos Kiklopas detachments belonging to the WCDS. Our observations show that skarn formation is associated with the activity of detachments and the coeval emplacement of the pluton. Endo and exoskarn deposits formed coeval with the ductile and brittle structures resulting from the activity of the WCDS, such as echelon veins, veins with antithetic shear and boudinaged veins wrapped within sheath folds, with a top-to-the SSW or SW shear senses compatible with the regional kinematics. Some skarn breccias formed within detachment planes far from the contact of the main granodioritic body, attesting for the intense flow of magmatic fluids along these discontinuities. These over-pressurized fluids play a major role in the mechanical behaviour of the detachments and strain localization. The two detachments acting as preferential crustal-scale drains, the pattern of magmatic fluid flows is not centred on the intrusion. In this context, iron-rich skarns and associated primary magnetite deposits have been remobilized during late brittle increments of motion along the detachments, together with surface-derived fluids responsible for deposition of the economic Fe/Ba mineralization. Finally, comparison with other mineralization type along the WCDS allows us discussing general features of metallogenesis associated with detachment faults in the Aegean.

Key words: Serifos, garnet-pyroxene endoskarns, pyroxene+/-ilvaite skarn breccias, detachment, granodiorite, strain localization.

1. Introduction

Fluid-rocks interactions during deformation are a major clue when addressing fault dynamics, especially for the formation of metamorphic core complexes (MCCs) and associated

detachment zones (here defined as gently dipping normal-displacement crustal-scale shear zones, e.g. Davis et al., 1986) for three main reasons.

Firstly, fluid pressure and fluid-rock reactions have major mechanical roles in initiation, propagation and long-lived slip of detachment zones (Reynolds and Lister, 1987; Sibson, 1985, 2000; Axen, 1992; Famin et al., 2004; Famin and Nakashima, 2005). In particular fluid overpressures and strain softening alteration reaction within fault rocks, partly explain the "weak" behaviour of detachments zones and the so-called mechanical paradox of low-angle normal faulting at initiation and propagation stages (Collettini, 2011 and references therein). This aforementioned author also argued that fluids overpressures coupled with the mechanical behaviour of alteration minerals in gouges would be responsible in part for the absence of moderate to large earthquakes along detachments zones; large amount of extension being then achieved aseismically.

Secondly, hydrodynamics and hydrothermal regime of such detachment zones and associated MCCs are directly controlled by multi-scale fluid-rock interactions and resulting permeability. The "classical" hydrodynamic model for MCCs and associated detachments corresponds to (Reynolds and Lister, 1987): i) an upper plate with hydrostatic surface-derived fluid pressure, free convective cells, high fluid-rock ratios under high differential stresses; ii) a lower plate with supra-hydrostatic metamorphic/magmatic fluid pressure, low fluid-rock ratios under low differential stresses. It is however well established that surface-derived fluids may deeply percolate at the brittle-ductile transition along detachment zones (Fricke et al., 1992; Kerrich and Rehrig, 1987; Famin et al., 2004; Mulch et al., 2006) triggering abnormal advective thermal gradients able to drastically refrigerate exhuming footwall rocks (Morrison et al., 1998). As they reach the top of the ductile crust, those surface-derived fluids are supposed to localize strain in a reaction-enhanced weakening front (Famin et al., 2004, Gueydan et al., 2003). Such models, which imply much localized convection cells along

detachment zones in the upper brittle crust, are quite different from the "classical" model (see above) as they argue for much more localized fluid flow and fluid-rock interactions. Moreover, it is noteworthy, as pointed by Famin and Nakashima (2005) that hydrodynamic models of detachment zones are not unique and they identified hot deep-seated metamorphic fluids expelled upward in the brittle crust along the seismogenic detachment of the Woodlarck basin in Papua New Guinea.

Thirdly, MCCs and detachment zones host numerous mineralization and ore deposits coeval with extensional thinning of the thickened crust. (Spencer and Welty, 1986; Myers et al., 1986; Smith et al., 1991; Beaudouin et al., 1991; Beaudoin and Therrein, 1999; Cashman and Elder, 2002; Maineri et al., 2003; Seidel et al., 2005; Holk and Taylor, 2007; Menant et al., 2013). Studying the interactions between fluid, rocks and deformation is then crucial when addressing such economic mineralized systems. Long (1992) proposed to distinguish epithermal base and precious metal deposits found in this context from detachment fault-related ore deposits whose formation is restricted to detachment dynamics only. This distinction could be also applied to Cu-Mo porphyries found in the Rhodope massif (e.g. Marchev et al., 2005). Recognized detachment fault-related ore deposits are generally characterized by (Long, 1992): i) various mineralization styles as Cu-Fe-Pb-Zn-Ag-Au polymetallic replacements and veins, Ba-F veins and Mn bedded and veins; ii) low grades and tonnage; iii) hosted within breccias and cataclasites, frequently in secondary faults; iv) a strong and pervasive K metasomatism; iv) fluid inclusion homogenization temperatures ranging 150 to 300°C.

Most of above cited studies dealing with fluid-rock interactions along detachment zones traced fluid flows through stable/radiogenic isotopes and fluid inclusion studies. In particular, with exception of few studies (e.g. Rossetti et al., 2007), it is surprising that the contribution of magmatic fluids is most of the time inferred only from isotopic ratios in mineralized (e.g.

Smith et al., 1991; Holk and Taylor, 2007) as in non-mineralized detachments (Wickham et al., 1993). Indeed, syn-detachment and syn-core complexes exhumation magmatism have been recognized for a long time (e.g. Crittenden et al., 1980; Denèle et al., 2011; Smith et al., 2011 and references therein) and a triggering effect of plutonism on MCCs formation has been advanced (Lister and Baldwin, 1993). As crystallizing plutons potentially constitute an important fluid source and develop their proper hydrothermal systems associated with strong metasomatism (e.g. skarns, thermal aureoles and related mineralization), direct mineralogical, petrological and textural records of such igneous fluids induced metasomatism is often lacking along detachment zones and associated core complexes. Moreover, outcrops of such pluton induced metasomatism/hydrothermalism close to detachment systems are necessary to understand the effects of fluid-rocks interactions on strain localization induced by magmatic fluid sources.

In this paper, we present a petro-structural study of the Serifos skarns integrated within the Aegean domain structural and geodynamic context. Serifos Island corresponds to a metamorphic dome where a synkinematic pluton emplaced alongside a detachment system (Grasemann and Petrakakis, 2007; Iglseder et al., 2008; Tschegg and Grasemann, 2009; Grasemann et al., 2012; Rabillard et al., 2015 and references therein). Analogue settings implying relations between skarns, granite and detachments have been studied in Elba Island (Rossetti et al., 2007), but fluid-rocks interactions were studied at small scale without accounting for large-scale detachment dynamics. As in Elba, the Aegean skarns are famous for their rich and spectacular mineralogy. These are observed on the Greek mainland, at Lavrion (Skarpelis, 2007; Voudouris et al, 2008; Bonsall et al, 2011; Berger et al., 2013, Spry et al., 2014) and on the Cycladic islands of Santorini and Serifos (Skarpelis, 2002). Iron (and baryum) mineralization was mined at Serifos in the 19th up to the beginning of the 20th century. Some of them are skarn-related, most of them appear to postdate major magmatic

pulse in first approximation. Mineralogy and petrology of the Serifos skarns and Fe/Ba mineralization have been accurately studied by Salemink (1985). However, this study did not address the link between magmatism and activity of the detachments, which were not yet identified at that time. Thus, favoured by the exceptional quality of rock exposures, Serifos appears to be a natural laboratory to depict igneous-driven fluid-rock-deformation interactions along detachment zones.

2. Geodynamic and Geological settings

2.1. Geodynamic of the Aegean Sea

Since the Late Cretaceous, the Africa-Eurasia convergence has led to the formation of mountain belts in the Mediterranean, such as the Alps, Rif, Betic, Apennines, Dinarides, Carpathians and Hellenides (Stampfli, 2000). Since the end of the Eocene (30-35 Ma), slab retreat has induced the formation of back-arc basins and the mountain belts formed earlier have collapsed, forming the Alboran Sea, the Ligurian-Provençal basin, the Tyrrhenian Sea, the Pannonian Basin and the Aegean Sea (Le Pichon and Angelier, 1981; Malinverno and Ryan, 1986; Royden, 1993; Wortel and Spakman, 2000; Jolivet and Faccenna, 2000; Faccenna et al., 2003; Jolivet and Brun, 2010; Guillaume et al., 2013).

The Aegean Sea belongs to the central part of the Hellenides-Taurides belt formed by the closure and accretion of several oceanic and continental areas (Bonneau and Kienast, 1982; Van Hinsbergen et al., 2005; Huet, 2010) before collapse in the back-arc context.

Active extension is presently mostly localized in the Gulf of Corinth and western Turkey (Armijo et al., 1996; McClusky et al,. 2000; Aktug et al., 2009; Pérouse et al., 2012). Since 5 Ma, the North Anatolian Fault (NAF) and its extension in the North Aegean Trough have

accommodated the westward motion of Anatolia (Armijo et al., 1999). Slab retreat and tearing have controlled the kinematics and localization of extension since the Oligocene (Figure 1a) (Jolivet and Brun, 2010; Royden and Papanikolaou, 2011; Jolivet et al., 2013; 2015).

Generally, three tectono-metamorphic units are recognized through the Cycladic islands within the Aegean domain (Bonneau, 1984). They correspond respectively to the Cycladic Continental Basement Unit (CCBU), the Cycladic Blueschists Unit (CBU) and the Upper Cycladic Unit (UCU).

The Cycladic Continental Basement Unit crops out in the central and southern parts of the Cyclades Islands on Naxos, Paros, Ios, Serifos and Sikinos (Andriessen et al., 1987; Grasemann and Petrakakis, 2007; Augier et al., 2015). This unit usually consists of granite, paragneiss and orthogneiss, and shows a complex pre-Alpine history attested by Hercynian and pre-Hercynian radiometric ages and relics of amphibolite-facies parageneses (Andriessen et al. 1987). Metapelites and marbles cape this basement unit and have been correlated with the Gavrovo-Tripolitza paleogeographic domain. Bonneau and Kienast (1982) have proposed that this unit corresponds to the Apulian southern margin of the Pindos Ocean and Jolivet et al. (2004) suggested that it extends in the continental basement of the Menderes Massif in western Anatolia. The Cycladic Blueschists Unit crops out on most islands of the Cyclades and is usually composed of a sequence of metapelites, metabasites and marbles. This unit belongs to the Pindos domain, corresponding to a basin of limited extension developed within Apulia with thinned continental and partly oceanic crusts (Bonneau and Kienast, 1982). The Upper Cycladic Unit consists of ophiolitic material partly metamorphosed by an HT-episode during the late Cretaceous. (Jansen et al., 1978; Maluski et al., 1987; Katzir et al., 1996).

The Cyclades are characterized by two tectono-metamorphic episodes: i) the first corresponds to crustal thickening in HP-LT conditions associated with the Eocene subduction of Apulia below the southern margin of Eurasia. This event is characterized by the growth of eclogite- and blueschist facies assemblages with radiometric ages ranging from 35 to 70 Ma (Altherr et al., 1979; Maluski et al., 1987; Wijbrans et al., 1988; Bröcker and Enders, 1999). Most ages are grouped between 40 and 50 Ma, corresponding to the Middle Eocene; ii) the second metamorphic event is related to post-thickening crustal thinning and HT-LP metamorphism during the Oligo-Miocene slab retreat episode (Altherr et al., 1982; Jolivet and Brun, 2010; Ring et al., 2010). Rocks underwent H/MT-LP metamorphism under greenschist and amphibolite facies, dated between 30 and 18 Ma from north to south of the Cyclades and it is associated with partial melting dated at 21-17 Ma in Naxos (Keay et al, 2001) or 16 Ma in Ikaria (Beaudoin et al., 2015). These rocks are exhumed in footwalls of MCCs (Lister et al., 1984; Buick, 1991; Urai et al., 1990; Gautier and Brun, 1994; Jolivet et al., 1994; Kumerics et al, 2005; Jolivet et al., 2010). At around 17 Ma, the southward migrating volcanic arc reached the Cyclades, yielding syn-tectonic igneous intrusion on the islands of Tinos, Delos, Mykonos, Ikaria, Serifos and Naxos (Alther et al., 1982; Faure et al., 1991; Tschegg and Grasemann, 2009, Bolhar et al., 2010; Rabillard et al., 2015; Laurent et al., 2015; Jolivet et al., 2015).

Exhumation is mainly accommodated by extensional shearing of the footwall along detachment zones often localized between the three units with a stretching lineation consistently oriented N or NE (Jolivet et al., 1994; 2013). Those tectonic contacts correspond to ductile shear zones and low-angle normal faults spanning the brittle-ductile transition. They have been identified in the northern and western Cyclades, and were respectively named the North Cycladic Detachment System (NCDS) and West Cycladic Detachment System (WCDS) (Figure 1a) (Jolivet et al., 2010; Lecomte et al., 2010 ; Iglseder et al., 2011 ;

Grasemann et al., 2012). On Sifnos Island extension was accommodated by high-angle to listric normal faults that may be a lateral extension of the WCDS (Ring et al., 2011; Roche et al., 2016)

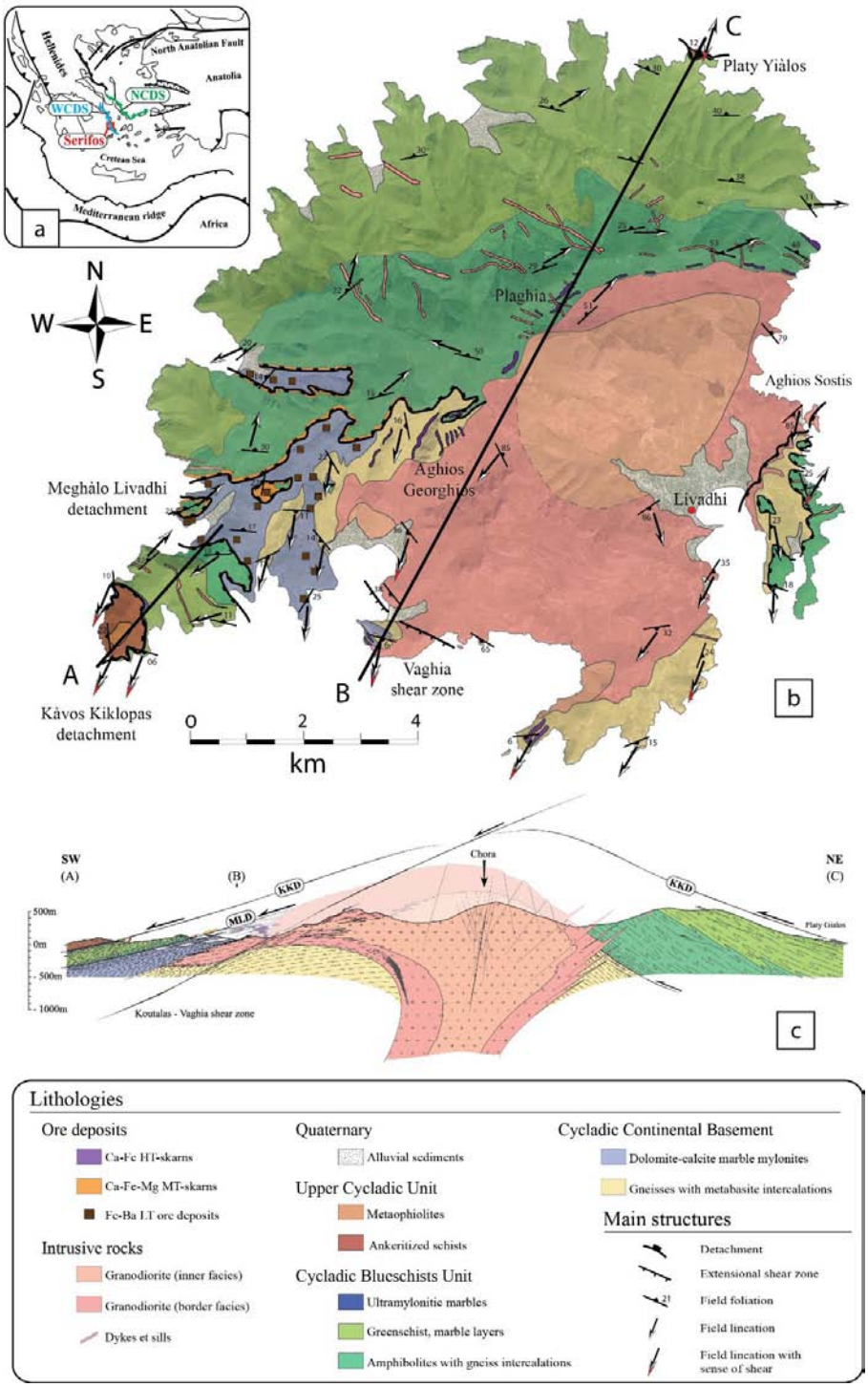

Figure 1: (a) Tectonic map of the Aegean region showing the main structures, the North Cycladic Detachment System (NCDS), the West Cycladic Detachment System (WCDS) and location of Serifos. (b) and (c) Geological map (modified after Marinos, 1951; Salemink, 1985; Grasemann and Petrakakis, 2007; Petrakakis et al., 2007 and Petrakakis et al., 2013) and SW-directed cross-section of Serifos (after Rabillard et al, 2015). MLD and KKD: Meghàlo Livadhi and Kàvos Kiklopas Detachments respectively. HT/MT/LT for respectively High, Medium and Low Temperature.

2.2. Geology and structure of WCDS on the Serifos Island

Serifos belongs to the Western Cyclades that form a NW-SE-trending alignment, between Kythnos and Sifnos (Figure 1a). The geology of Serifos consists of a granodiorite intruding the rearranged Eocene nappe stack (Figure 1b, c). On Serifos, the Eocene thickening event is characterized by a westward kinematic (sparse preserved W-directed lineations on Figure 1a) and was dated from 38 to 35 Ma ($^{40}Ar/^{39}Ar$ dating method on phengites [Schneider et al., 2011]). From base to top of the tectonic pile one finds (Grasemann et al., 2002): (1) the lowest structural unit composed of gneiss and massive mylonitic schists, less than 200 m thick, covered with calcite and dolomite mylonitic marbles. This unit belongs to the Cycladic Continental Basement; (2) the intermediate unit is composed of amphibolites at the base overlain by green-schists with marble intercalations. This unit occupying the northern half of Serifos shows rare glaucophane relics typical of the Cycladic Blueschists Unit (Salemink, 1985); (3) the uppermost unit is composed of marble and ankeritised protocataclastic shales. In the peninsula of Kàvos Kiklopas in the SW of Serifos a 10 meters thick serpentinite lens is exposed. These metamorphic units are described and displayed in a 3D model, implemented by the succession of units (see supplementary material n°1)

These units are separated by two detachments which both show top-to-the SSW kinematics (Figure 1 b, c). The Continental Cycladic Basement Unit-Cycladic Blueschists Unit contact crops out very well around Meghàlo Livadhi Bay and Cycladic Blueschists Unit-Upper Cycladic Unit interface intersects the Kàvos Kiklopas and Platy Gialos peninsulas (Grasemann and Petrakakis, 2007). Extensional deformation of the footwalls of the two detachments is marked by a NNE-SSW trending stretching lineation with top-to-the SSW

kinematic indicators. Both Meghàlo Livadhi and Kávos Kiklopás detachments (MLD and KKD respectively, Figure 1c) belong to the WCDS (Grasemann et al., 2012).

Serifos Island is thus interpreted as an MCC exhumed below the WCDS (Grasemann et al., 2002, Grasemann and Petrakakis, 2007), intruded by a I-type hornblende and biotite-bearing granodiorite (Ballindas, 1906; Ktenas 1917; Marinos 1951; Altherr et al. 1982). This pluton has two distinct facies (Salemink, 1985): the internal facies is a fine-grained equigranular unfoliated rock, while the enclosing external facies displays a mesoscale coarse grained texture, with large biotite flakes and many mafic enclaves. The pluton intrudes the MLD and the granodiorite roof is deformed by extensional shear zones in the south (Vaghia Bay) and east (Aghios Sostis) of Serifos. As illustrated by a 3D spatial modelling (see supplementary material, SM 1), the KKD is not intruded by the granodiorite main body, at least on the island. Both border and inner facies are interpreted as two successive intrusive pulses, emplaced during the WCDS activity (Figure 1c, Rabillard et al, 2015): the overall asymmetrical geometry and internal deformation argue for emplacement during a top-to-the-southwest non-coaxial flow from the magmatic stage to the sub-solidus mylonitic stage. The highest temperature of deformation is recorded by the recrystallization of K-feldspar (Tullis and Yund, 1977) in the extensional shear zone (Tschegg and Grasemann, 2009). At the periphery of the pluton, in the host-rocks, dykes and sills of granodiorite, microgranite and rhyodacite to dacite are widespread, especially in the western part of the island (Figure 1b).

This pluton intruded at shallow crustal level, across ductile-brittle transition (Marinos, 1951 Stouraiti et al, 2010) and, according to Salemink (1985), the lithostatic pressure at the time of intrusion was 1-1.5 kbar (i.e. 3.5-5.5 km assuming a 2.7 density). St. Seymour et al. (2009)

more recently estimated the pressure of crystallization of the core of amphiboles between 3.7 kbar and 2.5 kbar and the rims between 0.3 and 1.5 kbar (from 12 to 3 km).

The extensional deformation pervasively affects the Continental Cycladic Basement Unit and the Cycladic Blueschists Unit and also part of the granodiorite below the detachment in the south of the island (Grasemann and Petrakakis, 2007; Grasemann et al., 2012; Iglseder et al., 2009; Rabillard et al., 2015). According to the previous thermo-chronological data, the exact timing for ductile shearing along each detachment remains unclear since the extension-related retrograde greenschist metamorphism was partially erased by amphibolite-facies parageneses, likely induced by the granodioritic intrusion or by a more HT regional event (Iglseder et al., 2009; Grasemann et al., 2012). Nonetheless, available geochronological data (Rb-Sr on muscovite and biotite and TIMS U-Pb on zircon) yielded syn-greenschist mylonitization ages below the Meghàlo Livadhi detachment between circa 15 and 11 Ma while the granodiorite intruded the footwall of the Meghàlo Livadhi detachment between 11.6 Ma to 9.5 Ma (Iglseder et al., 2009) and underwent a fast cooling history together with the metamorphic dome until 4 Ma below the Kàvos Kiklopas detachment (Altherr et al., 1982; Hejl et al., 2002; Brichau et al., 2010; Grasemann et al., 2012).

2.3 Gitology and metallogeny of Serifos: data compilation and previous models

Serifos is well known to collectors for its spectacular skarn-related mineralization with gem quality in particular green quartz crystals with hedenbergite inclusions (prase or prasem). The island is also known for its numerous iron mines opened in: (i) numerous magnetite-rich skarns; (ii) hematite/limonite ± barite ore bodies in CCBU marbles that were exploited until 1963.

Marinos (1951) was one of the first authors to assign the highest metamorphic grade of the host rocks and skarns to contact metamorphism and metasomatism induced by the granodiorite intrusion. Salemink (1980, 1985) proposed a continuous hydrothermal model from magma emplacement an associated iron-rich skarns to Low Temperature (LT) Fe/Ba mineralization, in a classical context centred on a slowly cooling spheroidal pluton reacting with host rocks during thermal re-equilibration. This model is mainly based on a concentric zonation of skarns around the Serifos granodiorite: near the intrusion, skarns are mainly composed of garnet and pyroxene (hedenbergite and diopside) +/- magnetite at high-temperature (HT, between 560°C and 450°C), while at much larger distances from the intrusive body, skarns are massive and essentially formed by pyroxene at medium-temperature (MT, between 350°C and 260°C).

We compiled and plotted on synthetic diagram the $\delta^{18}O$ data from Salemink (1985) (SM2, supplementary material repository). Based on these data, and assuming reasonably high fluid/rock ratios for skarns, the HT and MT skarn formation of Serifos was achieved through fluids in isotopic equilibrium with the granodioritic magmatic waters. In contrast, isotopic signatures of LT Fe/Ba mineralization ($\delta^{18}O_{H_2O}$ on barite) strongly suggest a contribution of surface-derived waters enriched in ^{18}O.

Detailed mass balance calculations on Serifos skarns were also performed by Salemink (1985). The main result is that these skarns might be mainly issued from host-rock replacement (i.e. exoskarns) through percolation of metasomatic fluids deriving in part from the leaching of the granodiorite at the post-magmatic phase. Particularly, a large zone of "bleaching" within the granodiorite has been identified and is supposed to supply the major part of the Fe required to form the skarns. Oxygen Isotope data are compatible with such interpretation (SM 2). Later, such a bleached zone has been recognized by Tschegg and Grasemann, (2009) within the granodiorite in the hanging wall of detachment near Agios Sostis (Figure 1b, c). The extensive leaching of mafic components by pervasive fluid flow caused this bleaching of the granodiorite, with a much higher content of SiO_2, compensated by lower Al_2O_3 and CaO. This reflects the lack of Fe- and Ti-bearing and mafic minerals as well as the modal decrease of plagioclase (Tschegg and Grasemann, 2009).

Finally, when this previous model of skarn and associated mineralization deposition was established, geometrical and structural relations between the pluton, the host rocks and the succession of structures related to the two detachments were not studied nor integrated. Therefore, no model has ever been proposed to relate the formation of the skarn-related mineralization and the coeval deformation. Our study aims at filling this gap.

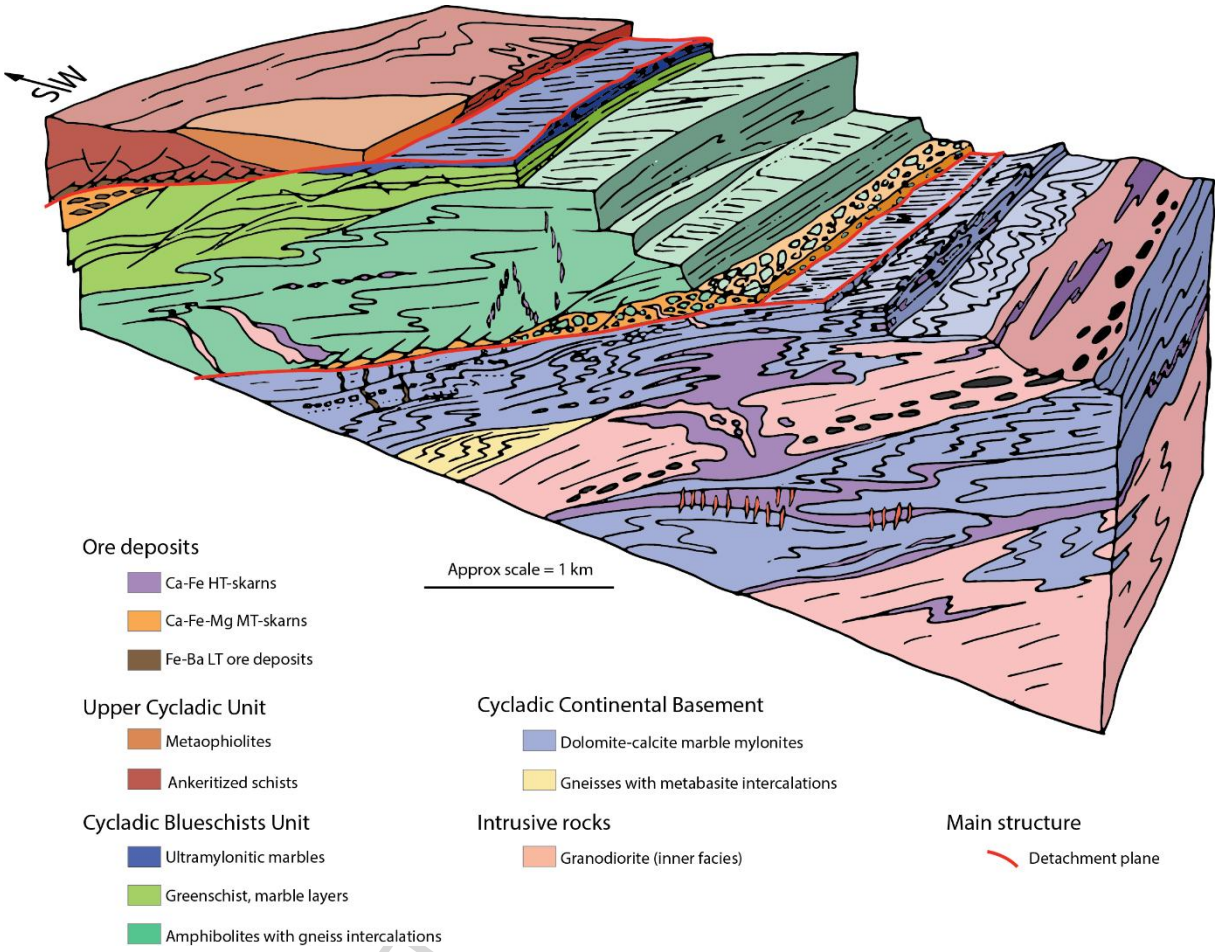

Figure 2: Three-dimensional diagram of SW part of Serifos summarizing the main lithostratigraphic units, both detachments and the structural position of different skarns.

3. Petro-structural typology of skarns and Fe/Ba-rich mineralization

In this section, we present a new petro-structural typology of the skarns reported on the geological map (Figure 1b and 2). In particular, we identified endoskarns and a regional skarn level never recognized before. Microscale textures are illustrated through thin sections microphotographs in supplementary material repository (SM 3, 4 & 5).

3.1. High-temperature skarns

All of those garnet-pyroxene HT skarns are proximal with respect of the granodiorite intrusion.

3.1.1. Massive garnet endoskarns in gneiss derived from the CCBU

These skarns occur in the Aghios Georghios area located in the centre of the island, in the Cycladic Continental Basement Unit just below the MLD near the contact between the gneiss (which contains sparse lenses of grey marbles) and the granodiorite (Figure 3). There, the contact with the granodiorite main body is sub-horizontal and parallel to the principal foliation. It is also characterized by numerous centimetric to decametric-thick intrafolial sill injections (Figure 3a). The skarns are mainly composed of garnet and form massive stratoid lenses subparallel to the principal tectonic foliation in paragneisses (Figure 3b, c, d), which can reach in places about 15 m in thickness (Figure 3b). Thus, they can easily be identified in the landscape by their reddish colour that contrasts with the lighter colour of gneiss. These massive garnet skarns contain essentially xenomorphic andradites, but occasionally euhedral garnets characterized by growth bands.

A retrograde paragenesis, marked by significant amounts of magnetite, is often observed in millimetre to centimetre-wide veins (Figure 3e), and can also reach significant proportions (up to 75 % vol. of magnetite), which justified their exploitation. Moreover, the skarn is recurrently intersected by millimetric to centimetric epidote-hematite veins and millimetre-thick quartz/actinolite veinlets. This retrograde phase is marked by veining of massive garnets filled with magnetite, hematite, epidote, actinolite, quartz and calcite.

Occurrences of these massive garnet skarns are consistently found parallel and within foliation of the hosting rocks, close to the contact with the main plutonic body. The lenticular morphologies of those skarns, occurrences of small sills of granodiorite incompletely skarnified (Figures 3c, d) and preservation of relict of magmatic minerals strongly argue for the metasomatism and replacement of magmatic sills and therefore define endoskarns.

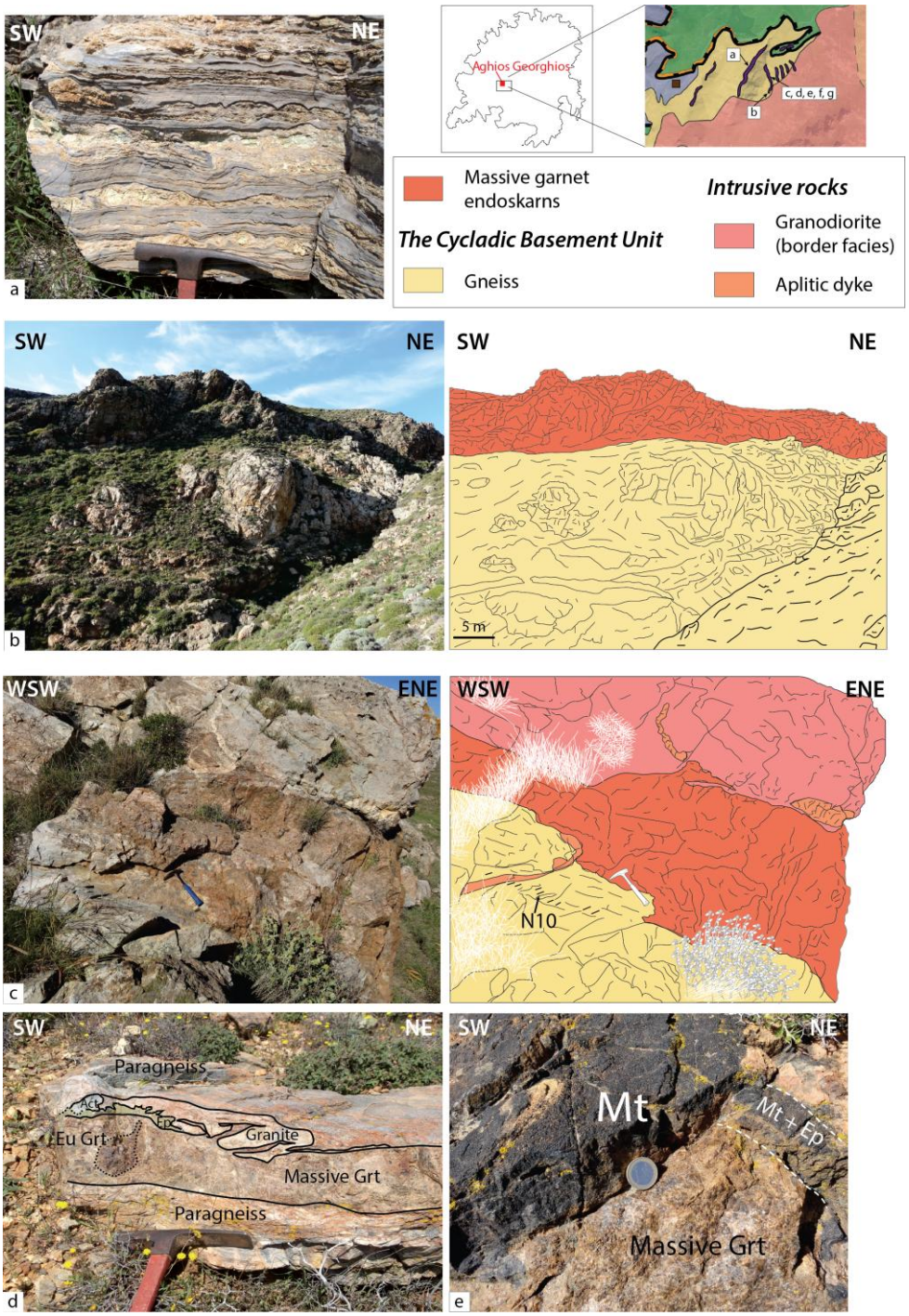

Figure 3: Massive garnet endoskarns in gneiss of CCBU, Aghios Georghios area (see location on figure 1). (a) intrafolial pegmatitic sills injected and boudinaged within gray marbles levels intercalated in gneiss of the CCBU. Pegmatites, derived from the Serifos granodiorite main body demonstrate the high exchange surface ratio between magmas and carbonates; (b) Panorama of one of the largest massive garnet endoskarn; (c) garnet endoskarn at the contact between gneiss and granodioritic sill; (d) massive garnet endoskarn outcrops; d) intrafolial sill in paragneisses replaced by massive garnet endoskarn. A magmatic quartz-feldspar assemblage of granitic sill (granite) is preserved at some place. Pockets of euhedral garnets (Eu Grt) and rim of retrograde epidote (Ep) and actinolite (Act) are frequently observed; e) magnetite (Mt) and epidote (Ep) veins within massive garnet endoskarn.

3.1.2. Garnet-Pyroxene endoskarns in marbles derived from the CCBU

Many occurrences of high temperature garnet-pyroxene skarn are found on the island, especially in the south near Vaghia Bay (Figure 4). The Vaghia outcrop is characterized by the presence of a ten-meter thick granodiorite (border facies) sill intruding an alternation of relatively pure grey and white marbles (Figure 4). The garnet-pyroxene skarns are found both inside the sill and at the interface with the host marbles (Figure 4). Two distinct skarn morphologies can be distinguished:

(i) "bubble" endoskarns: the first granular facies (Figure 4c) is found in the core of this granodioritic sill, sometimes as series of "bubbles" crossing the sill. The contact zone delimiting the skarn from the "fresh" granodiorite is diffuse and has many distortions and gulfs. Clasts of granodiorite preserved within the skarn (Figure 4c), indicate a partial metasomatism of the igneous protolith. These field observations are confirmed by thin-sections in which preserved and/or ghost of primary magmatic microstructures are found within the skarn mineral assemblage. Other replacement microstructures consist of hedenbergite rims growing around primary magmatic biotite and hornblende, and garnet rims around plagioclase (supplementary material 2). Therefore we qualified these skarns as "bubble" endoskarns.

The prograde assemblage of these endoskarns consists mainly of andradite (Ad_{90-80} Gr_{10-20}, Salemink, 1985) and hedenbergitic pyroxene (Hd_{20-40} Di_{80-60},), with vesuvianite ($Ca_{10}Mg_2Al_4(SiO_4)_5(Si_2O_7)_2(OH)$), a frequent sorosilicate in skarns, and wollastonite needles or rods. Garnets and clinopyroxenes are generally present in massive anhedral form although zoned andraditic garnets have been observed (Figure 4e). The amount of garnet is higher than that of pyroxene except for rare exceptions (Figure 4c).

(ii) “ribbon endoskarns”: the second facies is characterized by the formation of "ribbon" skarns plated under the upper marble contacts (Figure 4b). The skarn assemblage consists mainly of andradite garnet and minor hedenbergite but with a garnet-pyroxene alternation in some areas (Figure 4a, g). They are recognizable by their reddish-brown colour, and the presence of numerous vertical fractures (Figure 4b, f). Many evidences argue for the endoskarn origin: the contact skarn/white marble are sharp and wavy (Figure 4a) suggesting intrusive contact rather than fracture/open space contact with marbles; relicts of magmatic minerals are observed in thin sections within garnets; rounded and elongated clasts of granodiorite are preserved within skarn ribbons; meter to centimetre-thick skarnified sill intrude the marble foliation (Figure 4f) and are boudinaged by subsequent strain increment. Therefore, with exception of sparse garnets growing into marbles, ribbon skarns are endoskarns.

However, as sparse thin foliation-concordant and continuous skarns levels are encountered, we cannot rule out that thin beds of impure marbles have been metasomatosed into skarns. Anyway this type of skarns is poorly represented in outcrops at Vaghia.

In addition, within marbles, horizontal garnet veins (i.e. sub parallel to marble foliation, Figure 4g) have been observed in one location. In contrast, vertical garnet veinlets crosscutting ribbon endoskarns and granodiorite are widespread (Figure 4d). Noteworthy, these veins never cut the marbles.

In few locations, the “ribbon” prograde endoskarn minerals are partially or completely replaced by a retrograde phase mainly composed of magnetite (Figure 4h). This retromorphosis is usually found under the white marble. The mineralization has been exploited at the site in galleries, when the amount and grade were sufficient. Magnetite as the major phase is accompanied by pyrite, probably chalcopyrite (presence of malachite), actinolite, epidote, quartz and calcite. Clusters of talc and hematite form in places a particular

iridescent microstructure along magnetite bodies. This retrograde phase is generally pervasive. The initiation of this massive retrogression has progressed through fracturing preserved as frequent vertical magnetite veins, often associated with epidote/quartz veins and calcite veins. Vertical garnet veins intersecting the skarns are also observed crosscut by these retrograde veins. Importantly, as vertical garnet veins, these magnetite/epidote/calcite retrogression veins and magnetite stratoïd bodies are restricted to granodiorite sills and skarns; they have not been observed within marbles.

The granodiorite sill (border facies) shows many septa and basic enclaves along its base that is never skarnified even in contact with marble. Metasomatic reactions are thus observed only in the upper half of the sill, indicating upward fluid migration. A calcium-rich pegmatite with sphene, amphibole and hedenbergite occurs in the uppermost part of the sill just below the ribbon endoskarns. Sphene and amphibole belong to the main phase of magmatic intrusion, while the hedenbergite is derived from skarn processes. This suggests that the late- pegmatite parent magmatic liquid probably crystallized coeval with incipient metasomatic prograde reactions.

The last magmatic activity leading to skarn formation at Vaghia consists in a mafic dyke intersecting the entire outcrop (Figure 4). The dyke cuts across the white marble, granodiorite and tends to stop in the endoskarns. At the interface with marbles centimeter-thick garnet-pyroxene skarn shows that the mafic magma interacted metasomatically with marbles.

Finally, all lithologies are crosscut by vertical white veins and sparse normal faults filled with calcite and hematite ± barite. Ribbon skarns and grey marbles are also affected by a dense network of vertical joints.

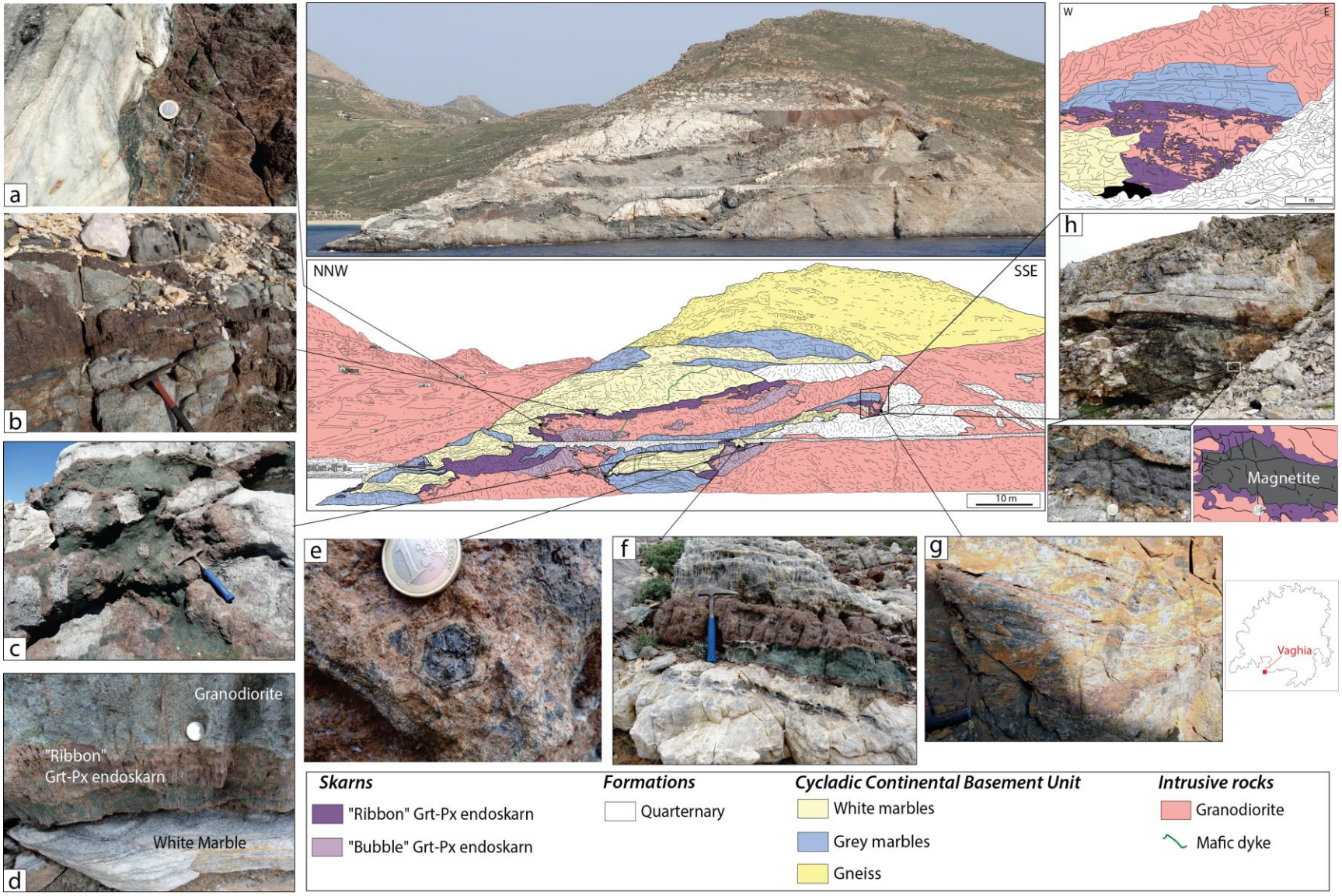

Figure 4: the Garnet-Pyroxene endoskarns in marbles of CCBU at Vaghia location, panorama and detailed outcrops. (a): sharp and wavy contact between marble and "ribbon" endoskarn; (b): typical microstructures and structure of garnet-rich "ribbon" endoskarns (reddish) developed within and at the top of the granodiorite sill (grey) just below the contact with white marbles; (c): typical "bubble" garnet and pyroxene endoskarns developed within the granodiorite sill in grey. Lobate clasts of granodiorite are preserved within skarn; (d): "ribbon" endoskarns developed within granodiorite sill, cross-cut by vertical garnet veins formed during the late prograde phase; (e): zoned euhedral garnet with alternating light- and dark bands; (f): decimeter-thick sill of granodiorite injected between fractured grey and white marbles and completely skarnified in the "ribbon" facies. Note the alternation of garnet (reddish) and hedenbergite (green) ribbons; (g): sub-horizontal garnet veins in grey marbles; (h): area mined for iron showing the skarn retrograde phase with magnetite +/- pyrite within ribbon endoskarns.

3.1.3. Fissural Garnet-Pyroxene exoskarns in amphibolites of CBU

Fissural garnet-pyroxene skarns outcrop at the Plaghia locality (Figure 1b) within the CBU along the northern edge of the granodiorite. These exoskarns are mostly observed within en-echelon vein arrays within amphibolites (Figure 5a, c, e), but also in veins parallel to the low-dipping main foliation and locally boudinaged (Figure 5b, d, f). Some horizontal veins also have vertical apophyses that cut the foliation (Figure 5d).

Most veins show a core of anhedral brown andradite with thin rim of bottle green hedenbergite, with a granoblastic microstructure typical of skarn. Some garnet-pyroxene veins are cut by vertical EW-trending cracks filled with quartz and the strike of these veins (Figure 5g). The retrograde phase is marked by epidote veins cross-cutting the entire outcrop (Figure 5b). Sparse malachite veneers are noticeable along a minor fault.

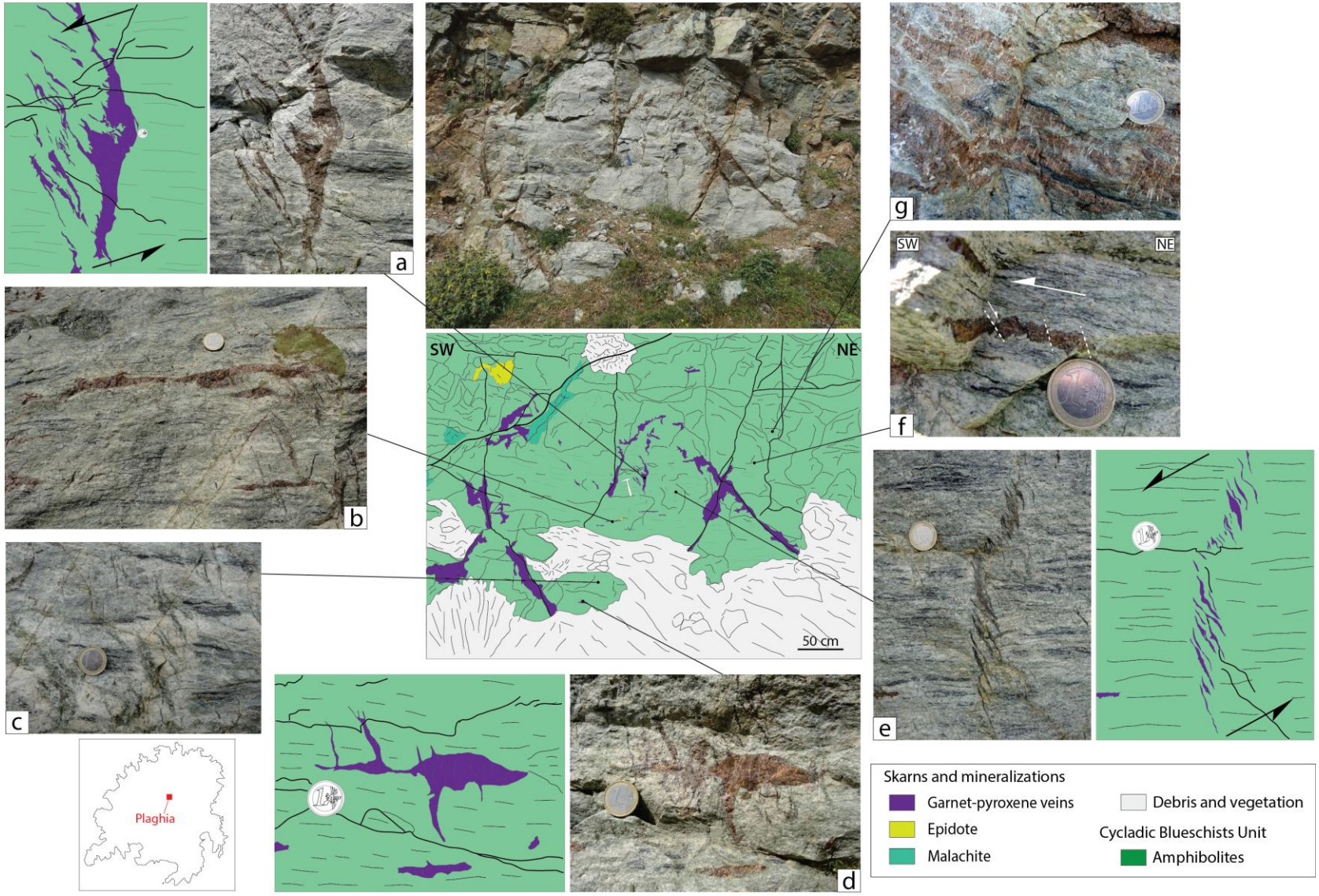

Figure 5: Fissural Garnet-Pyroxene exoskarns in amphibolites of CBU at the Plaghia outcrop. Although, the bulk skarn fracture pattern seems to indicate coaxial vertical shortening and horizontal stretching (e.g. through conjugate fractures), detailed kinematic criteria argue for a low amount of top-to-the SW simple shear. (a): en-echelon garnet veins indicating the top-to-the SW shearing; (b): veins mainly fill with garnet parallel to the foliation and cut by epidote veins; (c): en-echelon vertical pyroxene veins with a top-to-the SW shearing. (d): garnet vein parallel to the foliation with its apophyses intersecting the foliation; (e): en-echelon garnet veins indicating the top-to-the SW shearing intersecting the host-rock foliation; (f): boudinage of intrafolial garnet-pyroxene veins with top to the SW antithetic shears; (g): garnet veins parallel to the foliation truncated by small quartz veins.

3.2. Medium temperature exoskarns

Medium temperature skarns correspond to a pyroxene-ilvaite assemblage yielding formation temperatures between 350 and 260°C (Salemink 1985). These skarns are typically distal with respect to the main granodiorite body (Figure 1 and 2).

New field observations allow characterizing morphologies, structures of this type of exoskarns in relation with detachments. These skarns form stratiform breccia levels in the southwestern part of the island (Figure 1b). They are located along both MLD and KKD and may record several cataclastic events.

3.2.1. Regional level of pyroxene +/- ilvaite skarn breccia along the MLD

The pyroxene +/- ilvaite skarn breccia outcrops at the base of the MLD hanging wall (Figures 1 and 6). This skarn formed a regional reference level that perfectly traces the MLD in the western part of Serifos Island. It is developed within amphibolites of the CBU and restricted to areas where the MLD footwall is made of marbles of the CCBU. It is noteworthy that in the area of Aghios Georgios (Figures 1 and 3), skarn occurrences stop abruptly where CCBU marbles of MLD footwall thin and disappear.

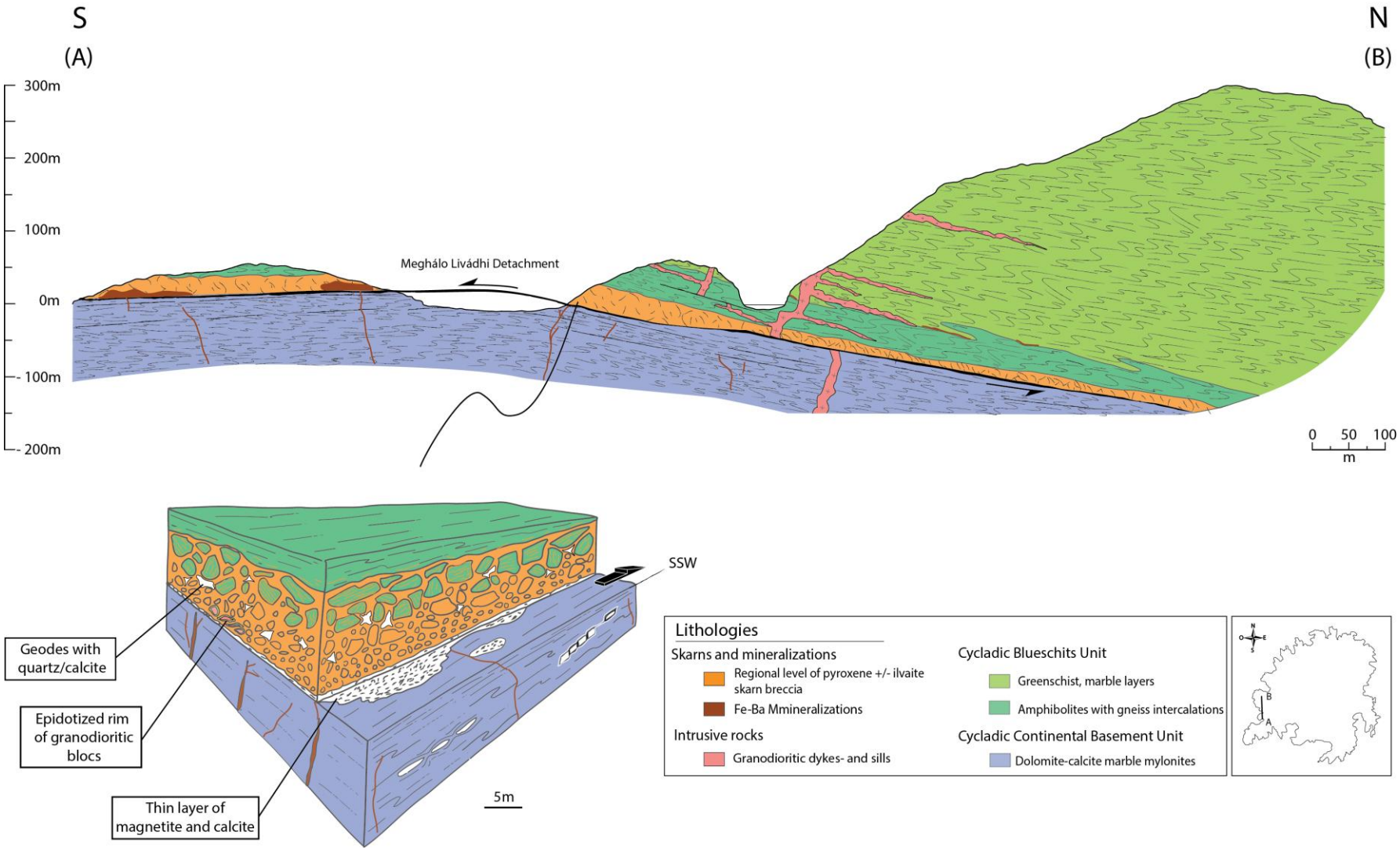

Figure 6: Interpretative geological cross section N-S oriented and crossing at Meghàlo Livadhi in the western part of the island. The Meghàlo Livadhi Detachment (MLD) and the regional level of pyroxene +/- ilvaite skarn breccia are represented. The 3D block shows the organization of this regional level at the Meghàlo Livadhi bay.

North of Meghàlo Livhàdi Bay, a spectacular outcrop of this regional level of pyroxene +/- ilvaite skarn breccia is presented on Figure 7. The breccia is composed with blocks of various sizes, up to several meters, and reaches a thickness of up to 30 meters (Figure 6 and 7). The skarn breccia lies abruptly over marbles of the CCBU localizing exactly the MLD plane. On marble mylonitic foliation, the MLD plane is platted by an undeformed thin layer of magnetite transformed into hematite and accompanied by calcite. Immediately above this layer the skarn level corresponds to a cokade breccia in which rounded clasts are cemented by geodes of skarn mineral assemblage or separated by cavities (Figure 7e, g). Amphibolite clasts, up to plurimetric size, are strongly skarnified as indicated by growth of concentric coronae around and within them (Figure 7e). The main prograde paragenesis includes pyroxene, specifically hedenbergite (Hd_{65-75}-Di_{35-25}) (Vergouwen, 1976), ilvaïte, epidote, calcite and quartz. The most abundant minerals are hedenbergite and ilvaite, which crystallize in the form of alternating monomineralic banding around and within clasts, while calcite and quartz fill with centre of geodic cavities that can reach plurimetric size. Ilvaite also crystallizes as geopetals in geodes (Figure 7g) and crosses them from side to side in some places. It also grows freely in the banding and may reach up to fifty centimetres size (Figure 7h). Microscopic study (see supplementary material) of the skarn breccia indicates that the first prograde mineral formed is epidote replacing primary protholitic microstructures and mineral assemblages. This massive epidotization is followed by development of veins, ribbons and bands of interdigitated hedenbergite and ilvaïte associated with quartz and calcite. The quartz is green at some place (“prase”) due to numerous hedengergite inclusions. In addition, associated with quartz, we found the presence of magnetite and pyrite, then retromorphosed into goethite by late oxidation stage. A subsequent retrograde phase is manifested by the development of fractures and veins with second generation epidote, calcite

and quartz. This assemblage filled the centre of geodic cavities and quartz show growth bands in very transparent euhedral prisms.

At this location, the level of skarn breccia presents a vertical zonation. As described above, the base is characterized by a cockade breccia with geodes and geopetals microstructures and complete replacement of clasts by hedenbergite/ilvaite banding, ribbons and rims (Figure 7e, g). Corrosion gulfs and coronae microstructures are diagnostic of chemical dissolution/corrosion mechanism during brecciation process. Upward from this basal cockade skarn breccia, the size of clasts increases up to meter-scale block (Figure 6 and Figure 7b, c, d) until the intact host amphibolite (Figure 7a). Clasts are less skarnified by the hedenbergite-epidote-ilvaite assemblage upward matching also the decrease of geodes occurrences. The internal foliation of these clasts indicates downward increasing component of block rotation within the skarn breccia level.

Numerous dykes and sills of granodiorite border facies outcrop above the skarn breccia level within the amphibolites and metapelites (Figure 7). In addition, granodiorite blocks are observed within the skarn breccia in the basal cockade facies (Figure 7f). Blocks distribution suggests they result from the dismemberment of a granodiorite sill. The blocks are massively epidotised at their periphery and are surrounded by hedenbergite-ilvaite coating, associated with geodic cavities. Epidotisation pervasively invades the granodioritic rock, migrating from edge to core of blocks. Thin sections show disseminated epidotes replacing primary magmatic minerals (amphibolites, plagioclase) with preserved shapes.

The outcrop of Meghàlo Livhàdi Bay (Figure 7) is an exception regarding the skarn breccia level thickness and its mineralogical expression. Regionally, the skarn breccia is thinner (5 to 10 m mean thickness), geodic cavities are smaller and sparse, and ilvaite is much less abundant than at Meghàlo Livhàdi Bay. The typical aspect of the breccia corresponds to a

crackle breccia with Ca-rich clinopyroxene veins and veinlets, sparse triangular geodic cavities, partly skarnified angular to rounded clasts and very low clast rotation component. This typical breccia facies is detailed in section below, as it is also encountered along the KKD.

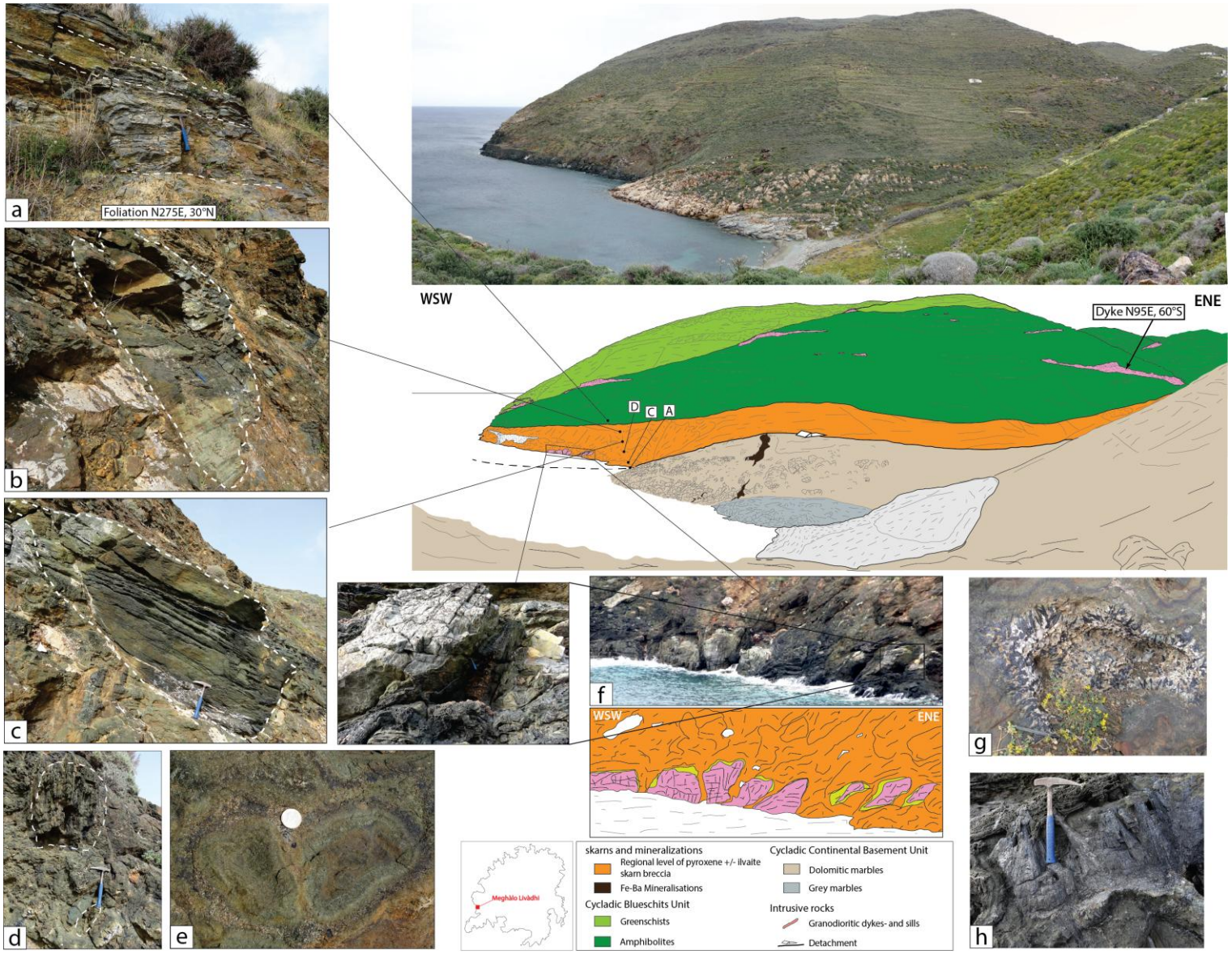

Figure 7: Panorama of Meghàlo Livadhi bay and the regional level of pyroxene +/- ilvaite skarn breccia. (a): amphibolite host-rock undisturbed and slightly metasomatosed; (b, c, d): upward sequence within the regional level of skarn breccia showing the increase of block size, decrease of block rotation and decrease of skarn metasomatism upward; (e): hedenbergite-ilvaite concentric banding around wholly skarnified clasts; (f): granodiorite blocs with epidotized rims at the base of the regional level of skarn breccia. Alignment of blocks suggests dismemberment of a granodiorite sill; (g): geodic cavities filled with quartz, calcite and radially-arranged ilvaite crystals (in black). Note the concentric metasomatic banding with alternation of pyroxene-rich (green) and ilvaite-rich (black) ribbons; (h): large size fibro radiate ilvaite crystals associated with radiating fibers of hedenbergite

3.2.2. Pyroxene skarn breccias along the KKD

The skarns morphology and facies present on Cape Kàvos Kiklopas is similar to that of the skarn breccia regional level along the MLD (Figure 8 and 9). However, the extension of this skarn is much more limited, only a hundred meters long and 3-5 meters thick. This skarn, which is structurally the highest of Serifos Island, is located at the footwall of the KKD and is limited to the north by a steep normal fault (Figure 8 and 9). As no skarn are found below the KKD in the northeasternmost part of the island (Plati Yiàlo location, Figure 1), it does not constitute a regional level of skarn breccia. At Cape Kàvos Kiklopas, the ultramylonitic marbles, overlying the CBU under most part of the UCU klippes, have been stretched and disappear, the skarn breccias lying directly on calcschists of the CBU (Figure 1 and 8).

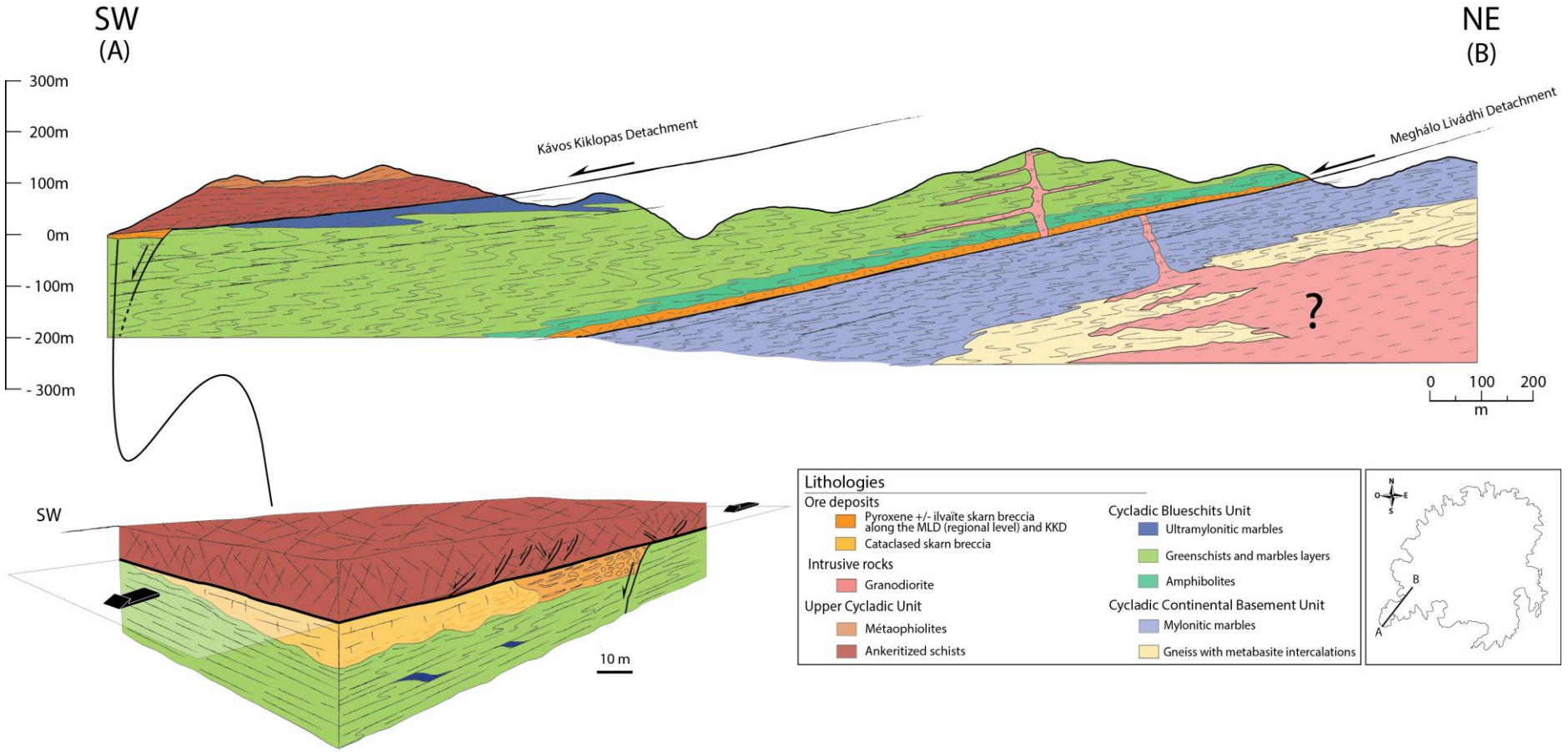

Figure 8: Geological NE-SW cross section in the southwestern part of the Serifos Island. The Meghàlo Livadhi- and Kávos Kiklopas Detachments are represented associated with the regional level of pyroxene +/- ilvaite skarn breccia. 3D bloc diagram represent detailed structures along the KKD at the Kávos Kiklopas Cape.

The skarn morphology evolves from north, next to the steep normal fault, to south toward the Cape Kàvos Kiklopas. The skarn develops initially in cokade and crackle breccias (dark orange in figures 8 and 9), with a large network of pyroxene veins, often horizontal, and triangular geodic cavities filled with large pyroxene crystals (diopside), calcite, quartz and hematite between rounded and skarnified clasts (Figure 9a, b, d). Remnants of ductile boudins surrounded by skarn deposits shows that the brittle deformation forming the cokade breccia was preceded by ductile deformation. Hematite is clearly a primary mineral and does not replace previous magnetite. Ilvaite is absent as well as magnetite. Pyrite and sparse garnets are also observed (Figure 9g).

To the south toward the cape, the skarn breccia is replaced by a green colored fine-grained cataclasite (light orange on Figure 8 and Figure 9f). The rock consists mostly of crushed pyroxene indicating that those rocks derived from catalasis of skarn. This cataclastic pyroxene skarns also contains a very fine-grained matrix similar to gouge granulometry. Rare garnets associated with interstitial euhedral calcite form clusters within the cataclastic pyroxene skarn (Figure 9g). The transition between the pyroxene skarn breccia and this cataclastic pyroxene skarn is marked by horizontal and vertical diopside veins that no longer constitute a real continuous network (Figure 9a, b). The retrograde phase is characterized by fractures filled with epidote crossing the cataclasite and crosscut by late cracks. Near the cape, the cataclastic pyroxene skarn tends to thin. Northward, the normal fault plane is marked by a black cataclasite, with a significant amount of pyrite disseminated or in veinlets and epidote veins attesting hydrothermal fluid flows through the fault.

Above the detachment (Figure 9c), the UCU consists of ankeritised and cataclastic schists associated with a low temperature iron mineralization, characterized by veins and pockets of hematite, calcite and +/- barite (Figure 9e).

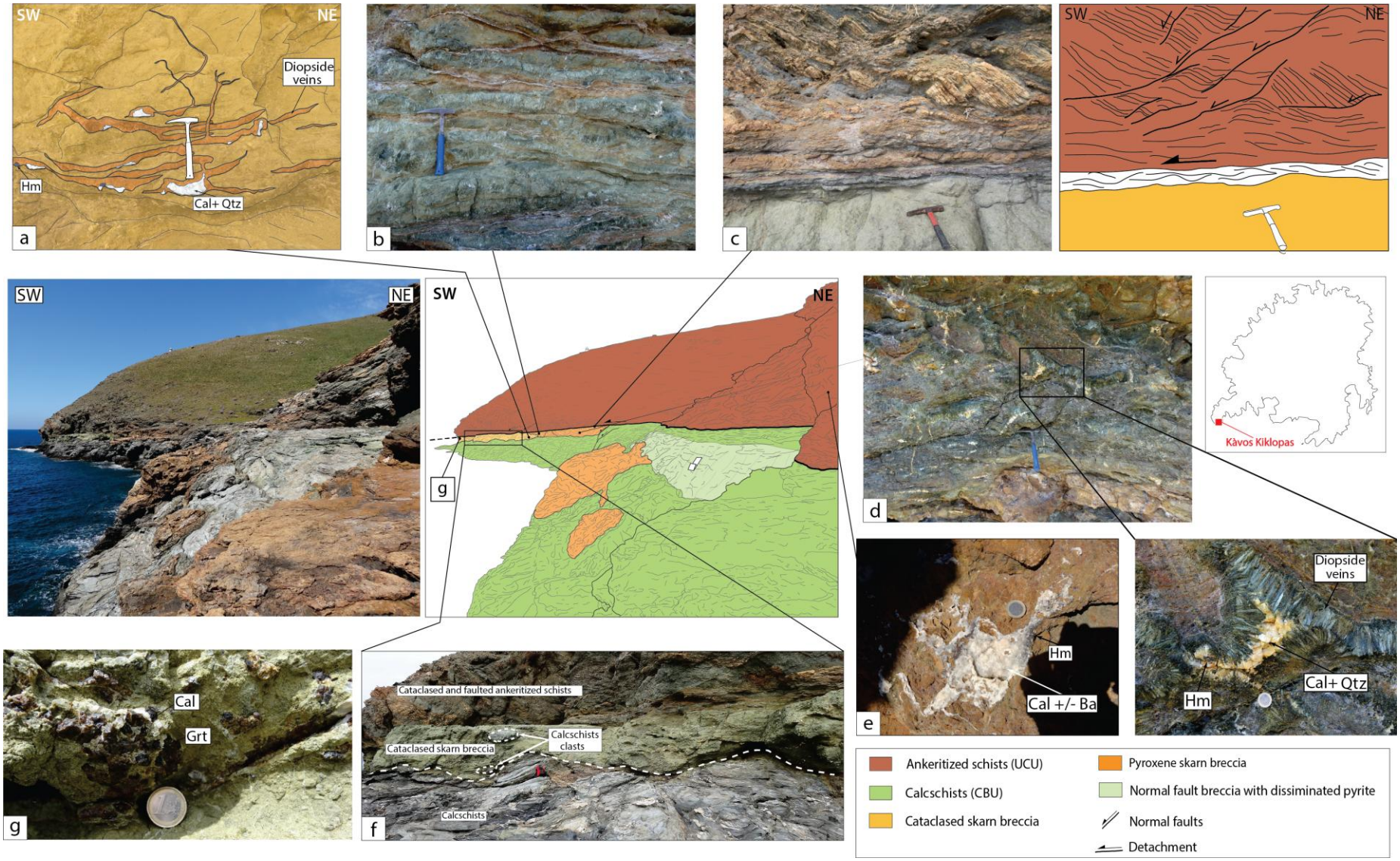

Figure 9: Exoskarns and breccias along the KKD at Kávos Kiklopas Cape. (a, b, d) : diopside veins and hematite, calcite and quartz geodes within the pyroxene skarn breccia. Note that most of pyroxene veins are flat lying; (c): the KKD is very localized between the cataclased skarn breccia and the ankeritized schists of the UCU as it is marked by a thin foliated gouge (in white on the line drawing); (e): hematite calcite, +/- barite and quartz veins within cataclased ankeritized schists; (f): the greenish cataclased skarn breccia incorporates clasts of the underlying calcschists unit (CBU); (g): Euhedral garnets and calcite preserved within the cataclased skarn breccia.

3.3. Fe/Ba LT mineralization

As mentioned above at Vaghia, skarn-related magnetite deposits provided very low tonnage of iron ore from exploitation quickly abandoned. The major part of iron concentrate came from ore containing hematite/limonite with barite. These mineralization are abundant and are found in all formations of the island above and below the MLD but often close to or within the regional level of skarn breccia (Figure 1 and 2).

In marbles from the CCBU the opening of cracks allowed the formation of banded veins generally consisting of hematite-limonite and barite (Figure 10a, b) and minor fluorite. Mineralized hematite-rich breccias are also observed within the regional level of skarn breccia forming large clusters. There are a few occurrences of these hematite/ barite breccias and veins in the amphibolites and metapelites of the CBU.

These Fe/Ba mineralization cut across all previously described units and clearly postdate the skarns. Paragenesis and microstructures are suggestive of a relative "cold" mineralizing environment. This is confirmed by Salemink (1985) who calculated a formation temperature of about 200°C for this late hydrothermal event. Possibly, part of the iron metal stock trapped within the regional level of skarn breccia, was remobilized by the late hydrothermal economic event.

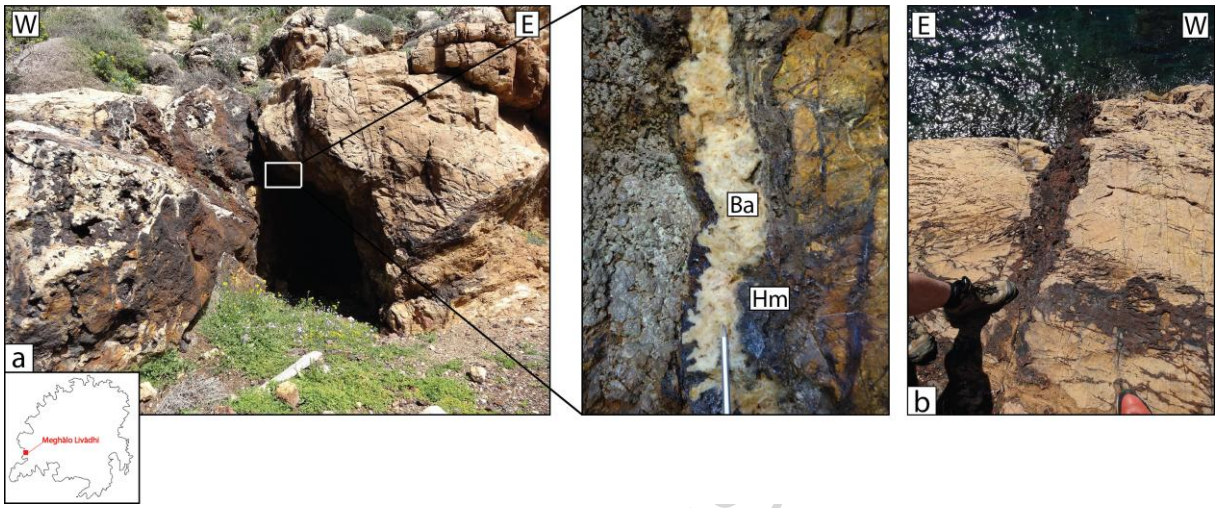

Figure 10: Hematite/limonite and barite mineralization of the Serifos Island. This mineralization represents the major mined ore of the island. (a): excavated hematite/limonite and barite veins and zoom on the vein. Wall rocks are dolomitic marbles of the CCBU; (b): View in the horizontal plane of the vein shown in (a).

3.4. Synthesis: paragenetic succession and skarn typology

HT skarns show a rather "classical" paragenetic evolution (Figure 11a) encountered in most of proximal metasomatic aureoles around intrusives in carbonated host-rocks (e.g. Meinert et al., 2005). A rough estimate of the garnet/pyroxene ratios yields values up to 50 for HT skarns. During the late prograde stage, an important fracturing event is responsible for the development of a dense network of vertical garnet veins. The magnetite ore (locally mined) associated with Vaghia endoskarns occurred at the beginning of the retrograde stage, which is also a common characteristic of iron skarns type (Pons et al., 2009). Garnet/pyroxene, the andradite/pyroxene/magnetite/pyrite association and the low amount of sulphides evidence that HT Serifos skarns are oxidized proximal skarns as defined in Meinert et al. (2005). Finally, in part due to low permeability of marbles, hydrous retrogression of skarns is only partial, most of the time restricted to epidote/quartz/actinolite veins.

MT skarn breccias present a "non-classical" and different paragenetic evolution (Figure 11b) from HT skarns marked during the prograde stage by early epidote crystallization, a very high

pyroxene/garnet ratio (garnet is absent in most outcrops) and ilvaite. Magnetite is poorly represented, the high iron content of MT skarns being included in calc-silicate minerals (epidote, hedenbergite and ilvaite). Ferric iron content in epidote and ilvaite demonstrates that the skarn is not as "reduced" as seems to be indicated by the high pyroxene/garnet ratio (Meinert et al., 2005). Regarding to HT skarns, the relative Al depletion in MT skarns and consequently the absence of grossular, might corroborate, together with decreasing temperature, the distal position from the intrusion that present Al contents much larger than amphibolitic skarn host-rocks. The hydrated composition of MT skarns calc-silicates (epidote and ilvaite) might also be explained in part by the high water content of amphibolites.

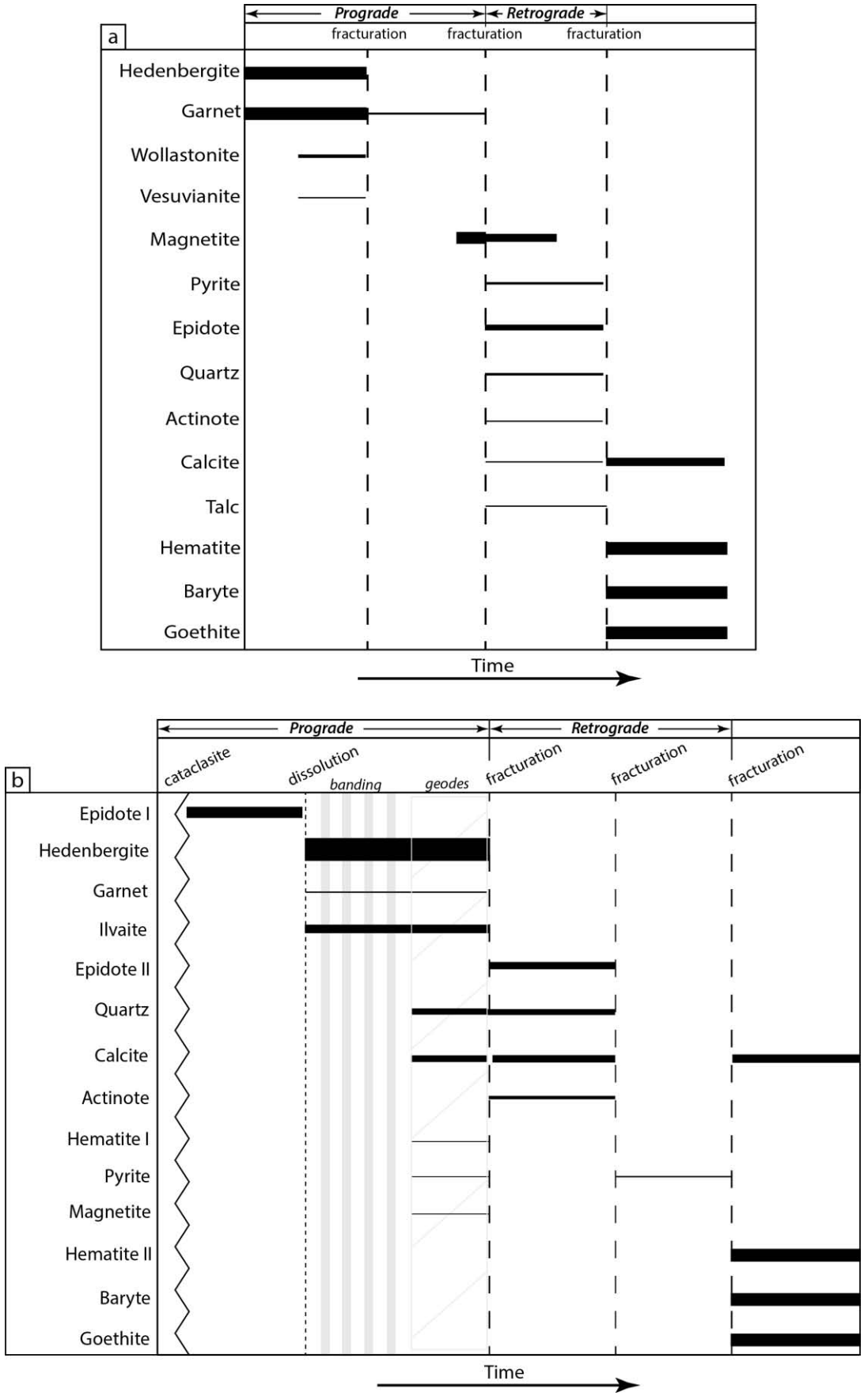

Figure 11: Paragenetic sequences of High Temperature (a) and Medium Temperature (b) Serifos skarns

4. Syn- and post-skarn deformation

4.1. Deformation of high temperature skarns

Ductile deformation is mainly observable were skarns developed within marbles of the CCBU at the Vaghia outcrop (Figure 12). Endoskarns, resulting from metasomatism of granodioritic sill injection, are more competent and underwent boudinage within the weak marble matrix (Figure 12). Skarn boudins are widespread in the western side of Vaghia location. Boudins are up to 1 meter in size at that place, likely resulting from deformation of thin skarnified sills rather than thick ones (Figure 12b, c). Skarn boudins are intimately linked and spatially associated with numerous non-cylindrical or sheath folds attesting for high non-coaxial localized strain (Figure 12b). It is noteworthy that some skarn boudins core isoclinal and sheath folds within the marbles (Figure 12a). Thus, on-going strain increments occurred after skarn metasomatism. Marble foliation bears a conspicuous N20°E horizontal stretching lineation parallel to the slightly SW plunging sheath fold axes (Figure 13e). In addition, in areas where regional strain rate is moderate (e.g. no sheath folds and mylonitization criteria), marble layers are often deformed and uplifted by magmatic volumic forces (i.e. ballooning). This is well illustrated by pegmatite and/or granodioritic sills stacking and further transformed into ribbon garnet and pyroxene endoskarns (Figure 3a, 4, 12). In host rocks as amphibolite from the CBU (e.g. Plaghia location on Figure 1), the fissural exoskarns are weakly affected by ductile deformation, with exception of sparse shear bands resulting in brittle asymmetric boudinage of intrafolial skarn veins (Figure 5f). Ductile internal strain within the granodiorite and skarns is less intense and is locally expressed by a discrete planar fabric marked by biotite flakes in granodiorite.

Brittle deformation in high temperature skarns corresponds to veins/veinlets and faults recording the prograde-retrograde-post skarn transition. At Vaghia, Plaghia and Aghios Georghios sites, the prograde skarn veins are: i) abundant sub-vertical N110E trending veinlets filled with garnet +/- pyroxene (Figures 4, 5, 12 and 13). Those are frequently en-echelon arranged (Figure 5); ii) intrafolial flat lying garnet and pyroxene veins re-opening host marble (one observation only) and amphibolite foliation and frequently connected to vertical garnet veins (Figures 4g, 5b and 13). Internal microstructure (see supplementary materials) and the lack of offset across these veins clearly demonstrate that both vein sets are pure extensional veins (i.e. mode 1 fracturing or "tension gashes"). However, this is partly accommodated by conjugate structures that accommodate local shearing. Retrograde veins mainly filled with epidote, magnetite and quartz show the same mean strike as prograde vertical veins (around N100E) but with higher variability of strikes and dips (Figure 13). Crosscutting former massive ribbon or bubble endoskarn, the retrograde veins may either re-open or crosscut former prograde veins (Figures 5). The fracturing mode of those retrograde veins is difficult to establish unequivocally. The late brittle event corresponds to hematite-quartz-calcite (± barite) veins, "dry" vertical joints and normal faults cutting all hosting rocks and skarns. Orientations of those late veins and faults is between N80°E and N100°E, i.e. parallel to former prograde and retrograde veins and normal to sheath folds axis and ductile stretching lineation within marbles (Figure 13).

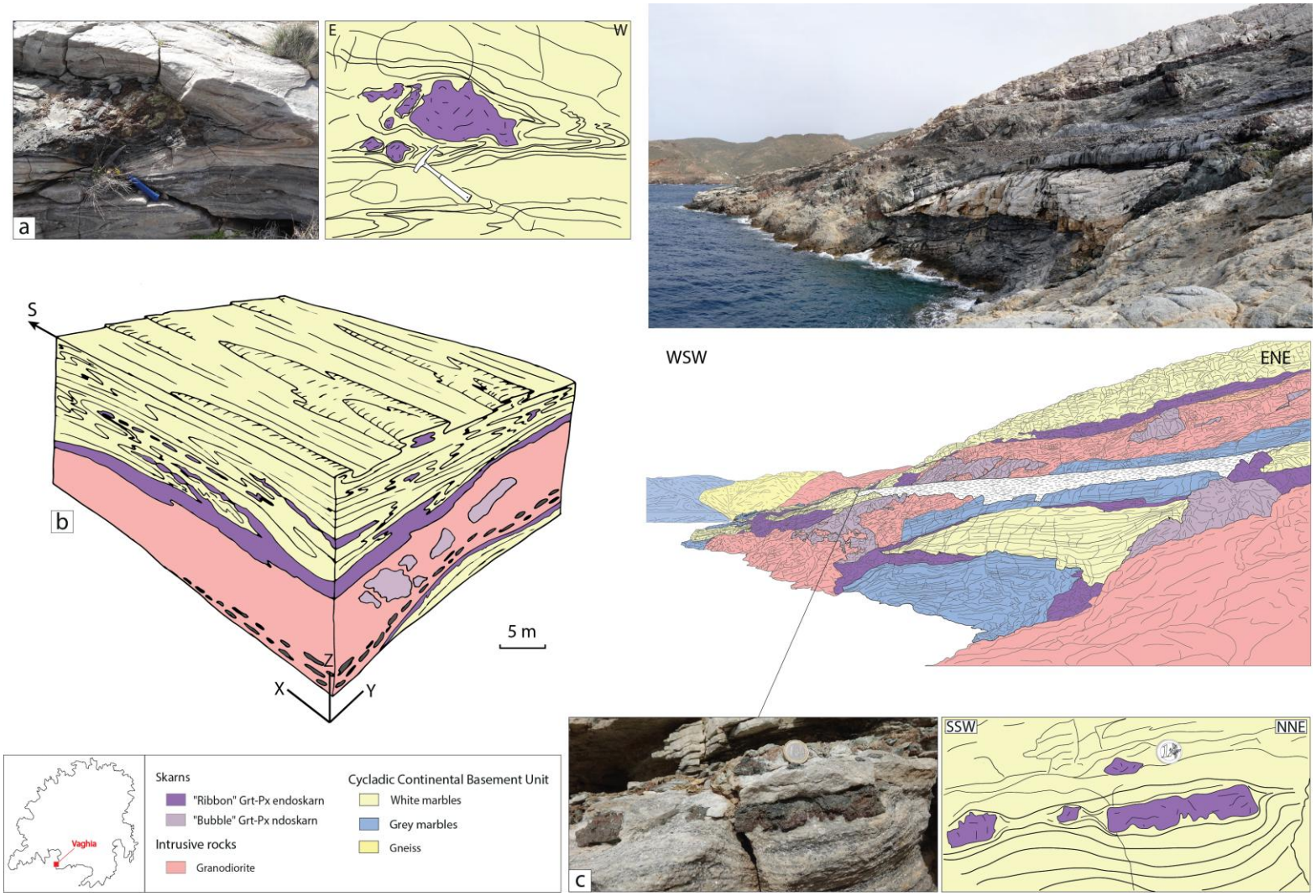

Figure 12: Deformation of Vaghia high temperature skarns. (a) sheath folds with endoskarn. (b) Three-dimensional diagram of boudins and sheath fold distribution. It summarizes the shearing strain distribution (c) thin skarnified sills boudins

4.2. Deformation of medium temperature exoskarns along the MLD and KKD

Ductile deformation around medium temperature exoskarns along MLD and KKD is only encountered within underlying ultramylonitic marbles/calcschists in which a subhorizontal NNE to NE-trending lineation is well expressed (Figure 13). Above the regional level of pyroxene +/- ilvaite skarn breccia along the MLD, amphibolites of the CBU bear the same stretching lineation. All kinematic indicators point to a top-to-the SSW shearing direction.

As described above, syn-skarn brittle deformation along MLD and KKD is accommodated by brecciation and veining. Associated with a strong replacement of clasts, open spaces and fractures are filled with skarn minerals forming crackle and cockade hydrothermal breccias.

At Meghàlo Livhàdi, dilatancy is large enough to induce rotation and collapse of meter-sized amphibolite blocks more or less skarnified. Interestingly, as hedenbergite and Ilvaite crystals in veins and cockade breccias are free of ductile deformation and cataclasis, this regional level of pyroxene +/- ilvaite skarn does not record major increment of slip along MLD after skarn metasomatism.

In contrast, the pyroxene skarn breccias along the KKD underwent further increments of brittle slip. The skarn was cut by the detachment during the last brittle increments also shown by the presence of clasts of hedenbergite veins in the cataclased skarn breccia (Figure 8 and 9). However, preserved Ca-rich pyroxene veins attest for episodes of hydraulic fracturing before frictional sliding and subsequent skarn brecciation (Figure 9a, b). Above a 10 cm-thick foliated gouge, deformation within the hanging wall of the KKD is intense and marked by normal sense C’ shear bands striking N110°E to N160°E roughly normal to the extension and branched to the foliated gouge (Figures 8 and 9c).

4.3. Synthesis of finite strain directions and kinematics recorded in skarn of Serifos

Figure 13 presents a synthesis of structural data collected at different skarn localities, including Platy Gialos where no skarn have been observed. The high-temperature skarns of Vaghia and Plaghia are located within the footwall and hanging walls of the MLD respectively (Figure 1). Those skarns unequivocally emplaced during a subhorizontal SSW-directed extensional regimes compatible with the WCDS activity (Figures 13b, e). Moreover, the transition from ductile structures (e.g. sheath folds and boudins around endoskarns, ductile stretching lineation…) to brittle strain (e.g. near vertical extensional veins filled with calc-silicates, en-echelon arranged at some place) spans the prograde/retrograde evolution of skarns. At Plaghia, en-echelon veins indicate a low amount of top to the SW shearing (Figure 5). The Vaghia skarn outcrops show high strains (e.g. sheath folds) developed within the marbles injected by granitic sills (Figure 12). This strain localization suggests that a major part of non-coaxial shearing is accommodated within heated and reacting marbles during and after skarnization.

In medium-temperature exoskarns localized along the MLD and KKD (Figures 13a, d), ductile and brittle deformations are compatible with general NNE-trending extension observed elsewhere on Serifos Island (Figures 1 and 13). Even though normal faults and shear bands within detachments show important dip variations, ductile kinematic criterias (e.g. asymmetric boudinage) unequivocally indicate a top-to-the SSW sense of shear. This non-coaxial deformation and associated top-to-the SSW kinematics is widespread and dominant in the island southern part (Figure 1 and 2).

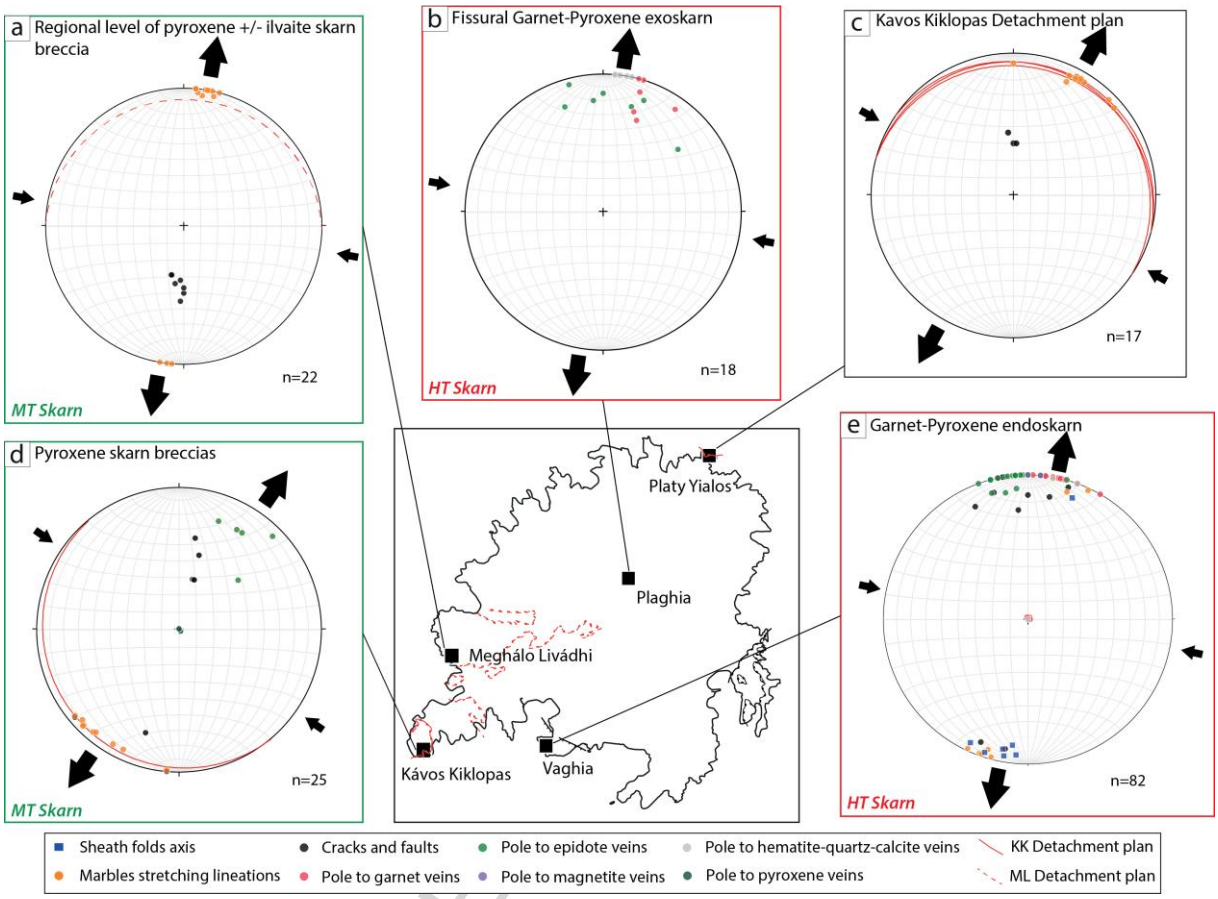

Figure 13: Synthesis of structural data related to syn- and post skarn formation of the Serifos Island. The Platy Gialos station where no skarns have been observed is added as it provides structural constraints for the Kàvos Kiklopas Detachment system (KKD). Stereograms in lower hemisphere.

5. Skarns, mineralization and detachments: interpretation and discussion

5.1. Fluid/rocks mass transfers with respect to previous model

The former model of Salemink (1980, 1985) emphasized that (see section 2.3 for detail): i) the proximal (HT) and distal (MT) metasomatic systems are buffered by magma-derived fluids, resulting in an isotopic depletion relative to metamorphic protoliths; ii) the Fe/Mg/Mn rich minerals in HT and MT skarns derived from fluids which leached in part those elements from the Serifos granodiorite during its cooling, resulting in a large zone of "bleaching" within the main pluton. During our field work, we recognized this zone of "bleaching" in the SW, where the granodiorite underwent unequivocal leaching of iron and concomitant Na metasomatism through albitization.

However, in contrast with Salemink works, we clearly evidence that a large part of HT skarn (garnet and pyroxene, more or less magnetite) are endoskarns and correspond to granodiorite sills metasomatic replacement rather than siliceous amphibolite/gneiss host-rocks metasomatism (e.g. massive garnet endoskarns at Aghios Georghios, Garnet/pyroxene ribbons and bubble endoskarns at Vaghia, Figures 1, 3 and 4). This interpretation weakens the gain and loss balance performed by Salemink (1985) that was only based on host-rocks replacement. We recalculate gain and loss from Salemink's data using a simple ratio between concentrations in elements (in ppm) of metasomatic rocks with respect to its protolith (density data are not available, so isocon-based methods cannot be applied). It shows that the HT skarnization of the granodiorite sill into a garnet/pyroxene assemblage would imply a huge gain of Fe (7.67), Mn (5.31) and Ca (4.92), immobility of Mg (1.01) and important loss of Si (0.56), Al (0.23), Na (0.01), K (0.10) and Ti (0.46). We suggest that those elemental losses are expressed within numerous pegmatites with titanite observed for instance at Vaghia. In that sense, we infer that skarnization of granodiorite sills injected within marbles is a "local" metasomatism at the sill scale and does not necessary require iron-rich fluids from distant

sources as the granodiorite pluton bleaching zone proposed by Salemink (1985). Furthermore, Ca gain resulting from marble decarbonatation through a complex process of carbonate assimilation by magmas, CO_2 incorporated into melts may trigger large variations in $f0_2$, fS_2 and volatiles content of melts (e.g. Iacono-Marziano et al. 2007, 2008, and 2009), hence promoting generation of iron-rich fluids and associated skarn processes.

Contrary to HT skarn, in agreement with Salemink (1985), the more distal MT skarns are exoskarns resulting from pervasive metasomatism of amphibolites and calc-shists and associated fracturing/sealing. Mass balance for the regional level of pyroxene +/- ilvaite skarn breccia along the MLD and the pyroxene skarn breccia along the southwestern section of the KKD yield Fe (1.77), Mn (2.73) gains and Na (0.05), K (0.03), Ti (0.01) losses. Iron-rich fluids thus percolated along detachment planes, likely from the granodiorite major body but also from numerous injected sills in the southwestern part of Serifos (e.g. the dismembered and altered sills outcropping along the MLD at Meghalo Livadhi Bay within the pyroxene/ilvaite skarns, Figure 7f). Calcium was likely supplied by proximal underlying marbles.

Low temperature Fe/Ba mineralization associated with hematite/limonite and barite depositions are mainly observed in calcitic marbles of the CCBU. This involves the addition of Fe, Mg, Mn in calcitic host-rock (i.e. widespread ankeritization of marbles), whereas Ca is extracted. These hydrothermal stages are accompanied with a strong addition of Ba forming the barite core of veins, as well as Cu, Zn and S (Salemink 1985).

5.2. Model of skarn formation in relation with deformation

Several lines of evidence suggest a different spatio-temporal scenario than the pluton-centred hydrothermal model proposed by Salemink (1985): i) HT and MT skarns never exhibit

crosscutting or overprinting relationships. MT skarns are not a retrograde evolution of HT skarns. In other words, both HT and MT skarns might be synchronous with the Serifos pluton construction and correspond to proximal and distal positions from the pluton contact. In the absence of geochronological data on skarns we favour this hypothesis; ii) MT skarns occur very far from the pluton contact (minimum of 2 km perpendicular to the contact, Figures 1 and 2) and are continuous along the MLD, i.e. the regional pyroxene skarn breccia we identified in this study. Indeed, even if "skarnoïds" are recognized without spatial connection with intrusives (e.g. Meinert et al., 2005, Li et al., 2014), skarns are generally restricted to the close vicinity of intrusion contacts (< 1 km). Therefore detachments in Serifos appear to be major drains for released magmatic fluids responsible for skarn deposition. The genetic model cannot be centred on the pluton as the interaction between the pluton and the detachments (Rabillard et al., 2015) have to be taken into account; iii) we identified numerous sills transformed into HT endoskarns not recognized in former studies (e.g. Figures 3 and 4). In the southwestern part of the island, granodiorite dykes and sills are widespread and some of them are in direct spatial relation with MT skarns (Figure 7f). This suggests that the pluton centred model and the concentric pattern of isotherm are not valid to explain skarn formation and repartitions. The sills injections and likely the construction mode of the main plutonic body (e.g. through a sill stacking mechanism, Menand, 2008; Michel et al., 2008) should also be considered when addressing spatial distribution of skarns and controlling isotherm patterns.

5.2.1. HT skarn genesis during detachment

In this section, we will focus on the Vaghia outcrops where skarn metasomatism and deformation are very well exposed. Figure 14 summarizes the HT skarn formation and fluid-rocks-deformation interactions prevailing during metasomatism. From Salemink (1985), we

assume a HT skarn formation depth around 5 km (Figure 14a). Based on the pluton architecture and the numerous sills observed, we suggest that the Serifos pluton grew through successive pulses of sill injections into favourable rheological interfaces such as the gneiss/marble contact in the Cycladic Continental Basement Unit (CCBU). This pluton emplacement mode controlled by rheological heterogeneities has already been documented and modelled (e.g. Roman-Berdiel et al., 1995).

Within marbles, magmatic sills and/or skarns localized ductile high strain zones (e.g. the sheath folds and spatially associated boudins of the Vaghia outcrop, Figure 12).

Firstly, to be interpreted, our data require a simple rheological model for marbles, discussed in the following lines. Indeed, our observations suggest that marbles behaved from a general brittle/ductile behaviour to a purely ductile one in the vicinity of sills and skarns (Figure 14). Temperature anomaly due to sill injection and/or large pluton emplacement is restricted to the close vicinity of magmatic bodies and is very quickly re-equilibrated with the regional thermal gradient (e.g. Eldursi et al., 2009 for plutons and Schenk et al., 2007 for thin sills). Therefore, as tectonic strain rates are much slower than magmatic injection/crystallisation rates (e.g. Paterson and Tobisch, 1992), we suggest that the pure ductile behaviour of marbles around sills and skarns cannot be only achieved through a single magmatic induced thermal anomaly, to explain the observed strain. In this context of metasomatism, this leads to consider rheological dependencies of interstitial fluid on calcitic rocks strength, paired with the effect of temperature. The “hydrolytic weakening” of fluids within calcitic rocks is still debated, in contrast with quartzitic rocks in which it has been demonstrated for a long time (Griggs, 1974). At temperature higher than 400°C, fluid assisted ductile weakening of marbles appears to be a minor effect from experimental works (i.e. whatever fluid pressure, marble yields always ductively above 400°C, Fischer and Paterson, 1989; Rutter, 1974; De Bresser et al, 2005), whereas it plays a major role for lower temperatures (<400°C, Liu et al.,

2002). Moreover, in contrast with those experimental works in which pore fluid is pure water or argon, natural percolating fluids implied in skarn formation are hot and very reactive hydrosaline and/or CO_2-rich chloride fluids (e.g. Fulignati et al., 2001). Thus, with such fluids, a reasonable assumption is that fluid-assisted weakening reactions at calcite grain boundaries exert important control on strain in natural marble-hosted skarns. Further microstructural, textural and isotopic studies will be necessary in the Vaghia marble to validate this point, but in first approximation we suggest that both increasing temperature in the close vicinity of granodiorite sill and percolation of skarn-forming fluid into marbles provide positive feedback to enhance ductile weakening of marbles (Figure 14a).

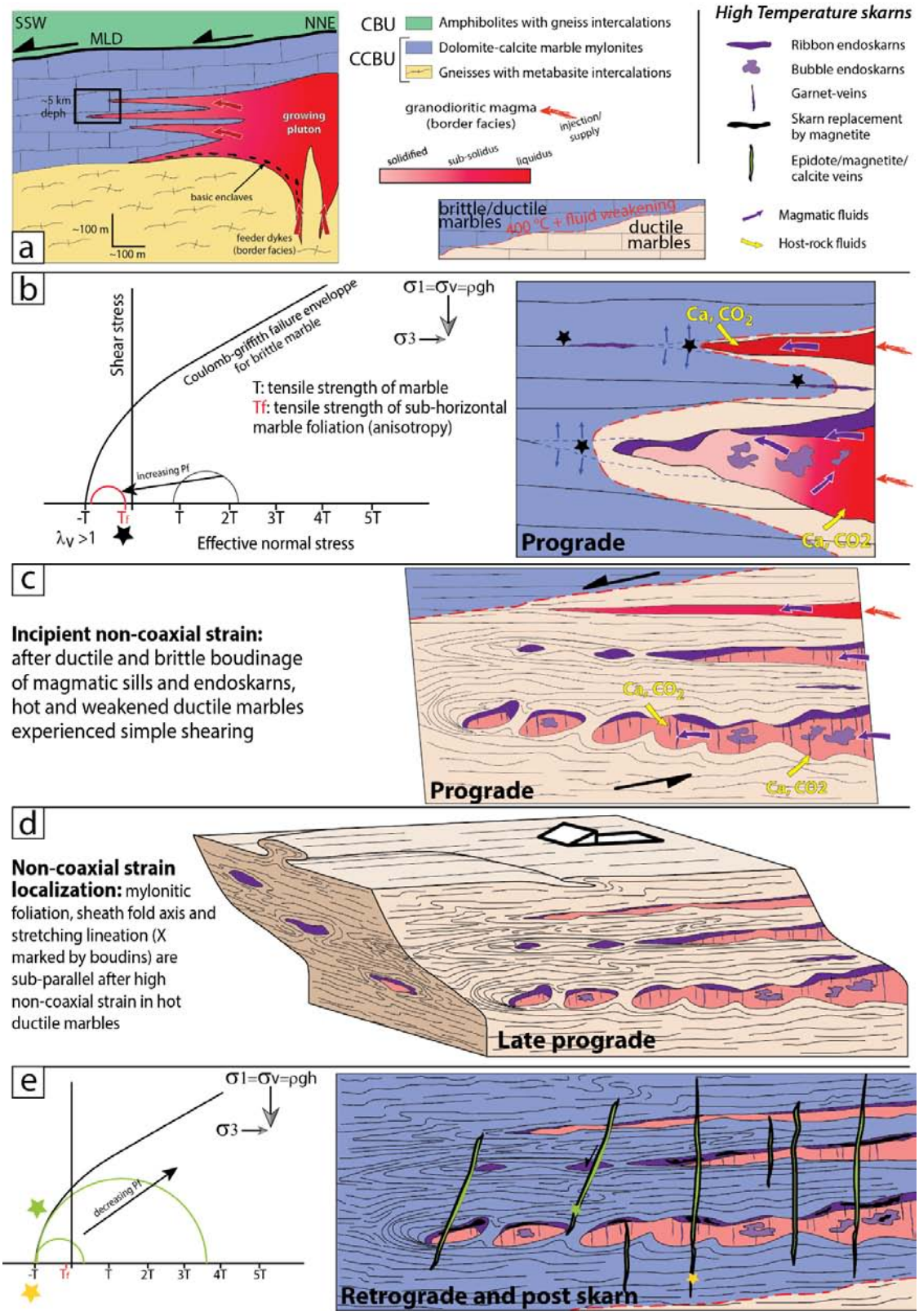

Figure 14: Synthetic model of the Serifos HT skarns formation in relation with detachment tectonics and sill injections. This model is based on the Vaghia skarn outcrops in the CCBU marbles. a) the Serifos granodiorite pluton is growing through sill injection/stacking mechanism within the CCBU marbles which act as a favourable rheological layer. Conjugated roles of temperature and metasomatic reactive fluids yield ductile weakening of

hosting marbles (see text for detailed explanation of rheological model); b) magmatic sills and foliation-parallel skarn veins propagate in brittle marbles through fracturing normal to regional σ_1 by opening of the foliation planes under high fluid pressure and low differential stress conditions; c, d) due to successive sill injections and subsequent skarnization, the ductile weakening of marbles lasts long enough to localized high strain non co-axial deformation related to extensional tectonics. A large part of MLD strain is then accommodated and localized; e) as temperature and fluid weakening decrease, embrittlement of marbles leads to the formation of extensional and hybrid shear/extensional retrograde skarn veins. The magnetite stratoïd bodies and veins formed during this stage. The Late LT Fe/Ba mineralization event is not represented. Noteworthy, among other explanation, the variation of differential stresses with fluid pressures (b and e) might be due to seepage fluid forces (see e.g. Cobbold and Rodriguez, 2007) and is well known in anisotropic rocks (e.g. Healy, 2009). MLD: Megalo Livadi detachment; CCBU: Continental Cycladic Basement Unit; CBU: Cycladic Blueschist Unit.

Secondly, using this rheological qualitative model for marbles, we proposed a multistage model for HT skarns formation during detachment. In a first stage (Figure 14b), granodioritic magma injected brittle/ductile marbles, horizontally "opening" the marble foliation. At 5 km depth, the lithostatic pressure roughly corresponds to 1.3 kbar and equal regional σ_1 in this extensional tectonic context. Sills "auto"propagate through fracturing localized at the sill tips and normal to σ_1. There, fluid pressures in marbles are high due to fluid infiltration/generation resulting from decarbonatation and on-going skarnization processes. Combined with magmatic overpressures, these fluid pressures are high enough to overcome locally and temporarily the lithostatic pressure and open foliation planes. Anisotropy of rock tensile strengths is likely a good candidate to explain extensional cracks parallel to σ_3 (i.e. opening of cracks parallel to σ_1): the tensile strength of horizontal foliation (Tf) is lower than the bulk tensile strength of an equivalent isotropic marble (T). This interpretation is reinforced by the foliation-parallel garnet veins observed in marbles (Figures 4g, 14b). Consequently, such interpretation implies low effective differential stress close to the tensile strength of isotropic marbles (in figure 14a, T is less than 10 MPa, Logan et al., 1993). The decrease of differential stress during an increase of fluid pressure in rocks has been recognized for a long time (Cobbold and Rodriguez, 2007) and is favoured in anisotropic rocks (Healy, 2009). Noteworthy, such mechanical interpretation (i.e. low differential stress and high fluid pressure) is also valid for HT fissural Garnet-Pyroxene exoskarns in amphibolites of CBU at the Plaghia outcrop (Figure 5). During this first stage, after magma injection within marble, as sills cooled and crystallized quickly, ribbon and bubble garnet/pyroxene endoskarns formed replacing granodiorite.

The second stage (Figure 14c and d) corresponds to non-coaxial strain localization in the areas where granodioritic sills injected into marbles. The pluton is still growing through sill injection mechanism and new sills are injected within marbles (Figure 14c). Ribbon and

bubble garnet/pyroxene endoskarns are still forming during crystallization of injected magmas. As the result, on-going weakening processes of marbles increase the volume of marbles behaving purely ductilely. Consequently, crystallizing granodiorite sills underwent ductile/brittle boudinage during progressing skarnization. Extensional garnet veins restricted to granodiorite sills formed at this stage (Figure 14c) cross cutting ribbon and bubble skarns. This weakening of marbles is then responsible for non-coaxial high strain localisation with sheath folds developed around boudins (Figure 14d). This deformation pattern and mechanism associating bulk simple shearing, boudinage and sheath folds is well described through analytical solution and analogue modelling by Cobbold and Quinquis (1980). Major difference with their works (cf. their Model 3) is that granodioritic and skarnified sills have a contrasting rheology relatively to marbles, sheath folds thus resulting from active folding around boudins.

In a last stage, cooling of the system resulting from the decrease of magmatic injection rate coupled with lowering of marble decarbonatation induces a broad embrittlement of marbles (Figure 14d). As a result, fluid pressure decreases within marble, which leads to failure from extensional fracture mode under very low differential stresses to hybrid shear/extensional fracture mode for larger differential stresses. Retrograde skarn fluids are trapped in those fractures filled with epidote/magnetite and calcite. The high porosity and permeability of coarse-grained ribbon and bubble endoskarns enhanced their replacement by iron-rich fluids. The main magnetite lenses, partly exploited, of the Serifos Island formed at this stage (Figure 14d). Not represented in Figure 14, later, the same brittle deformation occurred during LT Fe/Ba mineralization with extensional veins filled with barite and goethite and dry normal fault and joints.

Finally, our interpretation implies that the MLD is not only restricted and localized at the CCBU / CBU units interface. Indeed, the strain pattern observed indicates that at least the

entire thickness of the CCBU marbles is involved in a bulk simple shear. Injection of magmatic sill and subsequent skarnization with reacting fluids have localized high strain leading to heterogeneity of the simple shear at the marble unit scale.

5.2.2. MT skarn genesis during detachment

MT skarns formed from iron-rich magmatic fluids deriving from the granodioritic magmas and mainly replacing/fracturing amphibolites from the CBU along the MLD and KKD (cf. supra). Subsequent sill injections and stacking made the Serifos pluton grow (Figure 15a). In response to low permeability of deforming-recrystallizing marbles, we suggest that magmatic dykes and sills crossing the CCBU marbles/CBU amphibolites interface acted as major drain for magmatic fluids responsible for MT skarn deposition (Figure 15 b). The higher permeability in the MLD is likely related to a more brittle accommodation of extension in amphibolite compared to pure ductile flow within underlying marbles. This interface is thus a major discharge zone for magmatic fluids. Consequently, along this interface, fluid pressure increase coupled with a small differential stress state triggers two types of observed fracturing/reactivation (Figure 15 c): (i) firstly, episodic supra-lithostatic fluid pressure leads to re-opening sub-horizontal foliation planes within amphibolites. The tensile vertical strength of foliation planes is then reached and sub-horizontal veins filled with MT skarn paragenesis (mainly diopside/hedenbergite vertical fibers) formed near the MLD plane (yellow stars on Figure 15 c and d1). Channelized along normal faults, released magmatic fluids flow upward through the whole CBU unit and reach the low-permeability ultramylonitic marbles underlying the KKD plane (Figures 8, 9, 15b). As the result, following the same mechanical scenario as along the MLD plane, similar sub-horizontal Ca-pyroxene veins formed, opening foliation planes; (ii) secondly, high fluid pressures activate the MLD plane (i.e. interface

plane between CCBU marbles and CBU amphibolites (green stars on Figure 15 c and d1). This sliding increment yields dilatant cataclastic flow at the base of the CBU amphibolite unit leading to MT skarn assemblage deposition in veins network which forms crackle or mosaic breccias (Figure 15 d2). Following this interpretation, we suggest that this increment of brittle reactivation at the amphibolite unit sole, is responsible for the formation of the regional level of pyroxene ± ilvaite breccia. At some location, where its thickness is maximum, the regional level of pyroxene ± ilvaite breccia presents large dilatancy shown by clast rotation and large geodic cavities (e.g. the Meghàlo Livhàdi bay, Figure 7). Following Sibson (1986), we interpret such dilational hydrothermal breccia as relevant to dilational jog mechanism associated with hydraulic implosion brecciation (Figure 15 d). Such structures and associated hydrothermal breccia are poorly described and recognized in detachment systems. By increasing reactive surfaces, such brecciation process greatly favours chemical dissolution and replacement of clasts by skarn minerals during interaction with Fe-rich magmatic fluids. This is clearly evidenced by the rounding of clasts, and the concentric banding made of hedenbergite and ilvaite ribbons that may have entirely replaced the amphibolite clasts (Figure 15 d). Breccia formation ends with the filling of cavities by quartz and calcite, mostly. Therefore, this skarn breccia results from implosive mechanical hydraulic fracturing within dilational jog (Frenzel and Woodcock, 2014) probably combined with chemical brecciation processes as described in Lorilleux et al., (2000).

Finally, contrary to the regional level of skarn breccia along the MLD that does not record any strain increment after its formation, the skarn breccia formed below the KKD at the Kàvos Kiklopas cape has been cataclased and crushed during late brittle slip increment of the KKD.

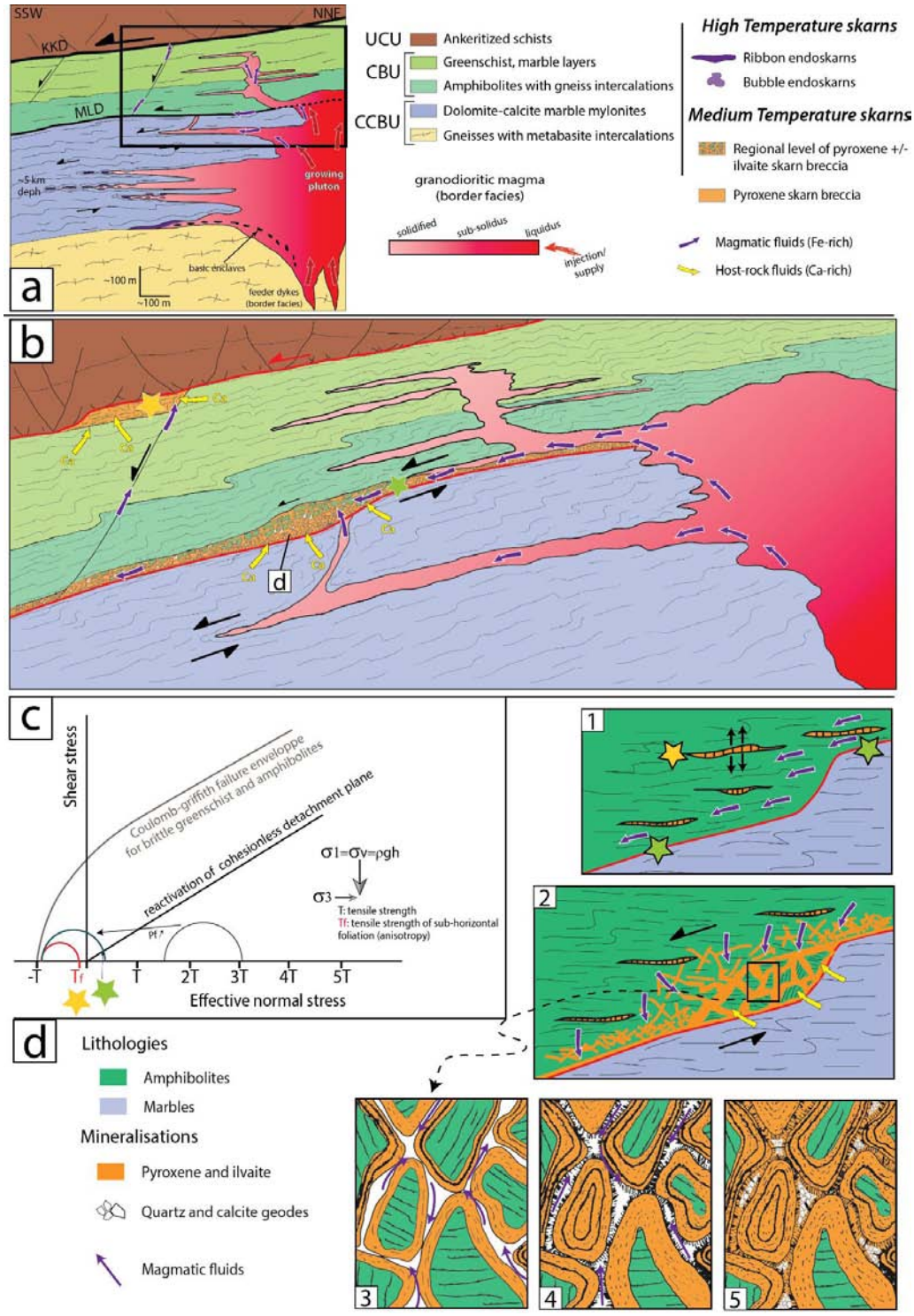

Figure 15: Synthetic model of the Serifos MT skarns formation in relation with detachment tectonics. a) on going pluton growth leads to pierce the MLD through dike and sill network; b) Inset in a, showing distribution along detachment of MT pyroxene rich skarn breccia. Marbles of CCBU acts as permeability barrier for magmatic fluids; c) mechanical interpretation of sub-horizontal foliation parallel skarn veins and detachment plane brittle reactivation; d) successive formation stages of the regional level of pyroxene +/-ilvaite skarn breccia with a focus on the Megalhi Livadi Bay location interpreted as dilatational jog. Se text for detailed explanation.

5.3. Implications on fluid flows and mechanics within the Serifos detachment system

The Serifos plutonic and the associated detachments system shows igneous-driven interactions between fluid, rocks and deformation along detachment zones. Figure 16 proposes a synthetic and simplified scenario of skarn and pluton emplacements during extensional continental thinning.

Firstly, through this study of skarns, magmatic fluids released from crystallizing magmas exert important controls on detachment mechanics and strain localization. Indeed, HT and MT skarns exhibit sets of prograde and retrograde skarn veins attesting for high fluid pressures, episodically supra lithostatic (Figure 14 and 15) and very low differential effective stresses. At the scale of a plutonic/metamorphic dome as Serifos Island, this strongly argues for an important mechanical role played by magmatic fluids in the brittle activity of detachments. In particular, along the MLD, the regional level of pyroxene/ilvaite breccia shows that mechanical effects and high magmatic fluid pressure may occur far from the plutonic main body (Figure 16 b). No further slip along the MLD has been recorded after this skarn breccia formation in Serifos, but we suggest that such magmatic fluid flow interplay with low-angle normal faults in the pluton vicinity. Moreover, we demonstrate that sill injection and subsequent HT skarnization within marbles are coeval with important ductile strain localization within marble units (Figure 14 and 16 a, b), where temperature increase combined to fluid weakening in marbles localized high shear strains. Although intuitive, this result has not been clearly observed and interpreted in other MCC implying marbles/metacarbonates and skarns (e.g Elba).

Secondly, the synkinematic Serifos skarns show that magmatic fluid flows may be efficiently drained into detachment (Figure 16 b) and that the circulation pattern of magmatic fluids in this detachment system is not centred and symmetric around the parental magmatic body. In

Serifos, fluid flows and pressure gradients are greatly controlled by the permeability barriers resulting from the vertical alternation of marbles/amphibolites/greenschists. Those different interfaces localizing detachments are crosscut by fluid pathways constituted by the numerous magmatic dykes and sills during pluton construction and by normal faults (Figure 1b). Such lithological alternations and the resulting permeability sandwich are common in MCC intruded by pluton (e.g. Tinos and Mykonos). Therefore, although skarns in Serifos are exceptional and are not generally the rule in other syn-extensional metamorphic domes, we suggest that the magmatic fluid flow pattern we depict in Serifos likely occurred in other MCC where a magmatic source is present.

Thirdly, the economic ore potential of such detachment/plutonic system (here the Fe/Ba concentrations in late veins) appears to be related to the last brittle increments of slip and fracturing (Figure 16 c) associated with on-going top-to-the SW extension. At this stage, fluids from surface flow downward into the system, likely yielding advective cooling and remobilizing skarns and magnetite deposits. As a result, deposition of mined Fe/Ba veins and stratoid bodies is then related to the late stage of brittle extension, a classical feature of mineralized MCC (cf. supra, introduction part). However, in Serifos, synkinematic iron-rich skarns and associated primary magnetite deposits formed important pre-concentration of iron, which explains why this island was the main Fe producer in the Aegean domain. Further mineralogical and geochemical studies dealing with remobilization of Fe-rich skarns and associated magnetite are required.

Finally, undoubtedly, the Serifos plutonic system and its associated skarns represent an exceptional example of a fossilized hypo-volcanic magma chamber in a detachment and back-arc extension context (Rabillard et al., 2015). Indeed, on one side, the well exposed dykes and sills network allows reconstructing the interdigitated architecture of the magma chambers with a very high specific reactive surface, and depicting mechanisms such as sill stacking for

example (e.g. Figure 16 a, b). On the other hand, skarns similar to those studied here could represent the origin of the skarn xenoliths sampled by volcanoes such as Mount Vesuvius, associated with a carbonate-hosted magma chamber (Fulignati et al., 2001).

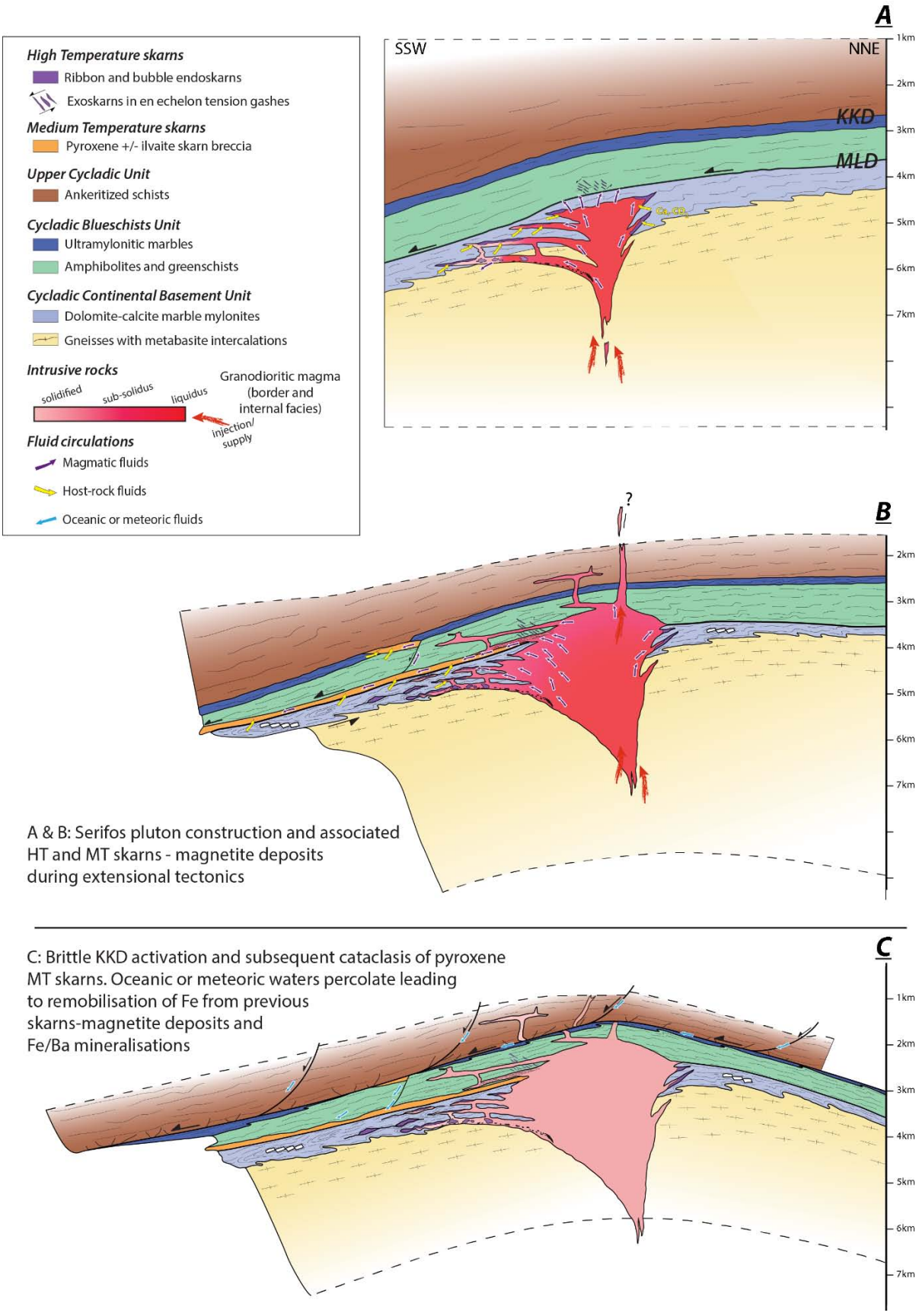

Figure 16: Synthetic model of the Serifos synkinematic skarns and pluton emplacement during post orogenic thinning in the Aegean domain.

5.4 Comparison with fluid systems and mineralization near the northern termination of WCDS at Lavrion.

Comparison between Serifos and the Lavrion mineralizing and fluid flow systems may be very instructive because both are located along the WCDS and are associated with Miocene intrusions in detachment context. The Lavrion mining district contains various different mineralization styles as porphyry-style mineralization (Voudouris et al., 2008; Bonsall et al., 2011), breccia-style mineralization (Economou and Sideris, 1976), skarn mineralization (Marinos and Petrascheck, 1956; Leleu et al., 1973; Economou et al., 1981) and finally economic Pb–Zn–Ag ore hosted in sparse veins or in strata-bound bodies within skarn-free replaced carbonate. In Lavrion area, the magmatism emplaced from 11 to 8 Ma (Skarpelis, 2007; Skarpelis et al., 2008; Liati et al., 2009), cooling ages yielding tectonic unroofing at 7.6 Ma (Berger et al., 2012; Altherr et al., 1982). As in Serifos, the Lavrion Miocene extensional tectonics is accommodated by top-to-the SSW detachment system that belongs to the northern termination of the WCDS (e.g. Skarpelis et al., 2008, Grasemann et al., 2012). The major detachment in Lavrion is equivalent to the MLD in Serifos, separating the basal continental unit made of marbles and schists in the footwall from the Cycladic Blueschist Unit in the hanging wall (e.g. Skarpelis, 2007; Marinos and Petrascheck, 1956 for tectono-stratigraphic mapping).

Porphyry, breccia, and skarn mineralization occur within or adjacent to the Plaka granodiorite and do not appear to be directly controlled by the detachment (e.g. no mineralization nor occurrences of these types are hosted within the LANF, Skarpelis, 2007; Berger et al., 2012). The skarns show classical prograde and retrograde paragenesis yielding formation temperature between 600° and 440°C at pressure ranging from 1.0 to 1.5 kbar (Leleu et al., 1973; Baltatzis, 1981). Locally skarns are “percolated” and replaced by massive

magnetite/pyrrhotite forming small stratoïd lenses in the close vicinity of the contact with the Plaka intrusion (Marinos and Petrascheck, 1956; Leleu et al., 1973; Economou et al., 1981).

In contrast, Pb-Zn-Ag carbonate-replacement stratoïd bodies and veins, which appear to be the most valuable ore in the district, are closely associated with detachment activity and associated normal faults (Berger et al., 2012). Fluid inclusion and stable isotope studies demonstrate that this mineralization is of "Manto-type" characterized by relatively high-temperature mineralizing solutions (>200°C) which derive from a magmatic source (i.e. the Plaka intrusion and associated dykes and sills) and interact with metamorphosed marine limestones through a high water/rock ratio (Berger et al., 2012; Bonsall et al., 2011; Voudouris et al., 2008; Skarpelis, 2007). As the result of the ductile/brittle evolution of the detachment, enhanced permeability allows magmatic fluids to flow far from the parent intrusion along the detachment.

Therefore, similarly to the regional level of MT exoskarns in Serifos, the Lavrion Pb-Zn-Ag carbonate-replacement mineralization also demonstrates that magmatic derived fluids are efficiently channelized along detachments. As in Serifos, rapid exhumation and late brittle slip increment are responsible for penetration of surface derived fluids able to remobilize previous magmatic-related ores and skarns, leading to economic and exploited concentrations of iron and baryum and potentially more economic metals within supergene gossan (Skarpelis and Argyraki, 2009). Finally, such magmato-hydrothermal systems associated with detachments appear widespread along the WCDS. Consequently, LANF have to be carefully considered when exploring metals in such context.

5.5. Implications for the interactions between intrusions, fluids and detachments in the Aegean domain

The Serifos granodiorite is part of a series of granitoid intrusions that emplaced during the Miocene from the Menderes Massif in the east to the west near Lavrion in a similar context. The oldest ones were formed in the east in the Menderes Massif (Catlos et al., 2010) and the eastern Cyclades (Ikaria, Laurent et al., 2015; Beaudoin et al., 2015) and the youngest ones further west in Serifos and Lavrion (Liati et al., 2009; Berger et al. 2013). This migration is likely due to the slab tear event that permitted the clockwise rotation of the Hellenides in the Middle Miocene (Jolivet et al. 2015). These intrusions have all interfered with crustal-scale extensional detachments (NCDS and WCDS) responsible for crustal thinning of the back-arc domain of the Hellenic subduction. The question of the relations between intrusions and the formation of detachments has long been debated (see for instance Lister and Baldwin, 1993). On the other hand, all these intrusions are emplaced into similar host rocks and yet, different types of mineralization have formed in association with these intrusions and no explanation has been so far proposed.

The formation of the Serifos skarn is contemporaneous with the intrusion of the granodiorite and the extensional deformation along the WCDS. The skarn and the subsequent economic Fe-Ba mineralization sign respectively the influx of magmatic and surface-derived fluids. The influx of surface-derived fluids occurred late in the evolution of the detachment system, after the interactions with magmatic fluids. On Tinos Island, where the intrusion was emplaced at greater depth, no significant mineralisation is observed, although the host rock is not much different, and fluids in the detachment are mostly meteoric in origin (Famin et al., 2005). On Ikaria, the situation is similar to Tinos with only very local skarn formation on a cm-scale, suggesting that magmatic fluids responsible for skarnification have not migrated far from the

intrusive contact. In Mykonos, a shallow intrusion, no significant skarn has developed and the economic mineralization is mostly barite in veins fed with meteoric or basinal fluids in a late stage of cooling, when the intrusion entered the brittle field (Menant et al., 2013). These different situations show that both magmatic fluids and meteoric fluids interfere with the formation of detachments in the whole Aegean. The case of Serifos is exceptional in the sense that magmatic fluids have penetrated the crust at a large distance from the intrusive contact in the ductile field and during exhumation and have interacted with strain localization along the contact. In Tinos (3,7-4,2 kbar Bröcker and Franz, 1994) and Ikaria (3-4 kbar, Laurent et al 2015) no such migration of magmatic fluids has occurred in the ductile regime, possibly because these intrusions were emplaced deeper than in Serifos, at higher temperature and thus in a more ductile regime where the porosity is not connected. In Serifos (3,7 and 2,5 kbar, St. Seymour et al., 2009) and Mykonos (1,5-5 kbar, Lucas, 1999), two less deep intrusions, a significant part of the late tectonic evolution occurred in the brittle field permitting the opening of large fractures (kilometric in the case of Mykonos, see Menant et al., 2013) and the penetration of surface-derived fluids down to the detachment footwall and the formation of the late economic Be-Fe mineralization. In Tinos and Ikaria meteoric fluids were always channelized along the detachment and no set of large kilometric fractures form that could have permitted fluid convection and mineralization. In Tinos it has been shown that meteoric fluids may penetrate the ductile-brittle transition along the detachment in a transient way during slip events (Famin et al. 2004b). This short review and comparisons suggest that the Aegean detachments are drains for both magmatic and meteoric fluids, magmatic fluids in the upper part of the ductile field and within the brittle-ductile transition and meteoric fluids above the brittle-ductile transition or within it in a transient way.

6. Conclusion

This work allowed us recognizing the different types of skarn and iron-barite mineralization exposed on Serifos island and their emplacement mode in relation with the intrusion of the Serifos granodiorite pluton below the WCDS. The interactions between magmatic fluids and the host rocks during deformation led to focusing ore concentration within the detachment plane and all lithological interfaces that are transposed parallel to the detachments during extension. The following types of ore deposits have been recognized:

(1) High-temperature skarns, characterized by garnet-pyroxene endoskarns and fissural exoskarns at the contact between the intrusion and the host-rocks.

(2) A regional level of medium-temperature brecciated pyroxene +/- ilvaite skarn along the Meghàlo Livadhi Detachment and also more locally above along the Kávos Kiklopas Detachment with normal faults connecting the two detachments and transferring metasomatic fluids upward.

(3) Iron and barite mineralization intersecting all formations and remobilizing the iron content from the former iron-rich skarns.

The entire skarn formation process and Fe/Ba mineralization is coeval with the activity of the two detachments which accommodate extension with top-to-the SW kinematics and the HT and MT skarns suffered ductile-then-brittle deformation along the detachment during their emplacement. Both the high-temperature and medium-temperature skarns formed during syntectonic pluton growth, whereas Fe/Ba mineralization occurred after pluton cooling and during last brittle increments of deformation within the exhumed Serifos metamorphic dome. The injection of magmas in the host tectono-metamorphic pile was controlled by the lithological alternation of gneiss, marbles, amphibolites and greenschists and drained into the detachments at long distance from the main plutonic body. During the formation of HT and MT skarns, fluids mostly came from the pluton, whereas the late low-temperature ore bodies

were deposited by meteoric fluids remobilizing the pre-concentrated iron mass of iron. The NCDS and WCDS are thus preferential channels of circulation for meteoric and magmatic fluids during the formation of the Aegean MCCs.

Acknowledgments

This work has received funding from the European Research Council (ERC) under the seventh Framework Programme of the European Union (ERC Advanced Grant, grant agreement No 290864, RHEOLITH) and from the Institut Universitaire de France. It is a contribution of the Labex VOLTAIRE. We are grateful to S. Janiec and J.G. Badin (ISTO) for the preparation of thin section, A. Menant, A. Beaudoin V. Roche and V. Laurent for many discussions on the Aegean domain and their constructive comments. F. Rossetti and anonymous reviewers have greatly improved the former manuscript versions as the editorial work of R. Govers.

References

Aktug, B., Nocquet, J.M., Cingöz, A., Parsons, B., Erkan, Y., England, P., Lenk, O., Gürdal, M.A., Kilicoglu, A., Akdeniz, H., Tekgül, A., 2009. Deformation of western Turkey from a combination of permanent and campaign GPS data: Limits to block-like behavior. J. Geophys. Res. 114. doi:10.1029/2008JB006000

Altherr, R., Kreuzer, H., Wendt, I., Lenz, H., Wagner, G.A., Keller, J., Harre, W., Höhndorf, A., 1982. A late Oligocene/early Miocene high temperature belt in the Attic-Cycladic crystalline complex (SE Pelagonian, Greece). Geol. Jahrb. E23, 97–164.

Altherr, R., Schliestedt, M., Okrusch, M., Seidel, E., Kreuzer, H., Harre, W., Lenz, H., Wendt, I., Wagner, G.A., 1979. Geochronology of high-pressure rocks on Sifnos (Cyclades, Greece). Contrib. Mineral. Petrol. 70, 245–255. doi:10.1007/BF00375354

Andriessen, P.A.M., Banga, G., Hebeda, E.H., 1987. Isotopic age study of pre-Alpine rocks in the basal units on Naxos, Sikinos and Ios, Greek Cyclades. Geol Mijnb. 66, 3–14.

Armijo, R., Meyer, B., King, G.C.P., Rigo, A., Papanastassiou, D., 1996. Quaternary evolution of the Corinth Rift and its implications for the Late Cenozoic evolution of the Aegean. Geophys. J. Int. 126, 11–53. doi:10.1111/j.1365-246X.1996.tb05264.x

Armijo, R., Meyer, B., Hubert, A., Barka, A., 1999a. Westward propagation of the North Anatolian fault into the northern Aegean: Timing and kinematics. Geology 27, 267. doi:10.1130/0091-7613(1999)027

Augier, R., Jolivet, L., Gadenne, L., Lahfid, A., Driussi, O., 2015. Exhumation kinematics of the Cycladic Blueschists unit and back-arc extension, insight from the Southern Cyclades (Sikinos and Folegandros Islands, Greece). Tectonics 34, 152–185. doi:10.1002/2014TC003664

Axen, G.J., 1992. Pore pressure, stress increase, and fault weakening in low-angle normal faulting. J. Geophys. Res. 97, 8979–8991. doi:10.1029/92JB00517wijbra

Baltatzis, E. (1981): Contact metamorphism of a calc-silicate hornfels from Plaka area, Laurium, Greece. Neues Jahrbuch für Mineralogie Monatshefte, 1981, 481-488.

Ballindas, I., 1906. The island Seriphos. Its geological construction and metal occurrences. Bull. Phys. Soc. Athens 1, 58–74.

Beaudoin, A., Augier, R., Laurent, V., Jolivet, L., Lahfid, A., Bosse, V., Arbaret, L., Rabillard, A., Menant, A., 2015. The Ikaria high-temperature Metamorphic Core Complex (Cyclades, Greece): Geometry, kinematics and thermal structure. J. Geodyn. doi:10.1016/j.jog.2015.09.004

Beaudoin, G., Taylor, B.E., Sangster, D.F., 1991. Silver-lead-zinc veins, metamorphic core complexes, and hydrologic regimes during crustal extension. Geology 19, 1217–1220. doi:10.1130/0091-7613(1991)019<1217:SLZVMC>2.3.CO;2

Beaudoin, G., Therrien, R., 1999. Sources and drains: Major controls of hydrothermal fluid flow in the Kokanee Range, British... Geology 27, 883.

Berger, A., Schneider, D.A., Grasemann, B., Stockli, D., 2013. Footwall mineralization during late Miocene extension along the west Cycladic detachment system, Lavrion, Greece. Terra Nova 25, 181–191. doi:10.1111/ter.12016

Bolhar, R., Ring, U., Allen, C.M., 2010. An integrated zircon geochronological and geochemical investigation into the Miocene plutonic evolution of the Cyclades, Aegean Sea, Greece: Part 1: Geochronology. Contrib. Mineral. Petrol. 160, 719–742. doi:10.1007/s00410-010-0504-4

Bonneau, M., Kienast, J.., 1982. Subduction, collision et schistes bleus : exemple de l'Egée. Bull. Société Géologique Fr. 24, 781–791.

Bonneau, M., 1984. Correlation of the Hellenide nappes in the south-east Aegean and their tectonic reconstruction. Geol. Soc. Lond. Spec. Publ. 17, 517–527. doi:10.1144/GSL.SP.1984.017.01.38

Bonsall, T.A., Spry, P.G., Voudouris, P.C., Tombros, S., Seymour, K.S., Melfos, V., 2011. The geochemistry of carbonate-replacement Pb-Zn-Ag mineralization in the Lavrion District, Attica, Greece; fluid inclusion, stable isotope, and rare earth element studies. Econ. Geol. Bull. Soc. Econ. Geol. 106, 619–651. doi:10.2113/econgeo.106.4.619

Brichau, S., Thomson, S., Ring, U., 2010. Thermochronometric constraints on the tectonic evolution of the Serifos detachment, Aegean Sea, Greece. Int. J. Earth Sci. 99, 379–393. doi:10.1007/s00531-008-0386-0

Bröcker, M., Enders, M., 1999. U-Pb zircon geochronology of unusual eclogite-facies rocks from Syros and Tinos (Cyclades, Greece). Geol. Mag. 136, 111–118.

Bröcker, M., Franz, L., 1994. The contact aureole on Tinos (Cyclades, Greece). Part I: field relationships, petrography and P-T conditions. Chem. Erde-Geochem. 54, 262–280.

Buick, I.., 1991. Mylonite fabric development on Naxos, Greece. J. Struct. Geol. 13, 643–655. doi:10.1016/0191-8141(91)90027-G

Catlos, E.J., Baker, C., Sorensen, S.S., Cemen, I., Hancer, M., 2010. Geochemistry, geochronology, and cathodoluminescence imagery of the Salihli and Turgutlu granites (central Menderes Massif, western Turkey); implications for Aegean tectonics. Tectonophysics 488, 110–130. doi:10.1016/j.tecto.2009.06.001

Cashman, S.M., Elder, D.R., 2002. Post-Nevad detachment faulting in the Klamath Mountains, California. Geol. Soc. Am. Bull. 114, 1520.

Cobbold, P.R., Quinquis, H., 1980. Development of sheath folds in shear regimes. J. Struct. Geol. 2, 119–126.

Cobbold, P.R., Rodrigues, N., 2007. Seepage forces, important factors in the formation of horizontal hydraulic fractures and bedding-parallel fibrous veins (’beef’ and “cone-in-cone”). Geofluids 7, 313–322. doi:10.1111/j.1468-8123.2007.00183.x

Collettini, C., 2011. The mechanical paradox of low-angle normal faults; current understanding and open questions. Tectonophysics 510, 253–268. doi:10.1016/j.tecto.2011.07.015

Crittenden, M.D., Coney, P.J., Davis, G.H., 1980. Cordilleran metamorphic core complexes. Geol. Soc. Am. 490.

Davis, G.A., Lister, G.S., Reynolds, S.J., 1986. Structural evolution of the Whipple and South mountains shear zones, southwestern United States. Geol. Boulder 14, 7–10.

De Bresser, J. H. P., Evans, B., and Renner, J., 2002, On estimating the strength of calcite rocks under natural conditions, in de Meer, S., Drury, M. R., de Bresser, J. H. P., and Pennock, G. M., editors, Deformation Mechanisms, Rheology and Tectonics: Current Status and Future Perspectives: London, Geological Society Special Publication, v. 200, p. 309–329.

de Bresser, J.H.P., Urai, J.L., Olgaard, D.L., 2005. Effect of water on the strength and microstructure of Carrara Marble axially compressed at high temperature. J. Struct. Geol. 27. doi:10.1016/j.jsg.2004.10.002

Denele, Y., Lecomte, E., Jolivet, L., Lacombe, O., Labrousse, L., Huet, B., Le Pourhiet, L., 2011. Granite intrusion in a metamorphic core complex; the example of the Mykonos Laccolith (Cyclades, Greece). Tectonophysics 501, 52–70. doi:10.1016/j.tecto.2011.01.013

Dill, H.G., Melcher, F., Kaufhold, S., Techmer, A., Weber, B., Baeumler, W., 2010. Post-Miocene and Bronze-Age supergene Cu-Pb arsenate-humate-oxalate-carbonate mineralization at Mega Livadi, Serifos, Greece. Can. Mineral. 48, 163–181. doi:10.3749/canmin.48.1.163

Economou, M., Sideris, C., 1976. A mineralized brecciated granodiorite porphyry in the Laurium mines, Greece. Neues Jahrb. Fuer Mineral. Abh. 128, 209–218.

Economou, M., Skounakis, S., Papathanassiou, C., 1981. Magnetite deposits of skarn type from the Plaka area of Laurium, Greece. Chem. Erde 40, 241–252.

Eldursi, K., Branquet, Y., Guillou-Frottier, L., Marcoux, E., 2009. Numerical investigation of transient hydrothermal processes around intrusions; heat-transfer and fluid-circulation controlled mineralization patterns. Earth Planet. Sci. Lett. 288, 70–83. doi:10.1016/j.epsl.2009.09.009

Faccenna, C., Jolivet, L., Piromallo, C., Morelli, A., 2003. Subduction and the depth of convection in the Mediterranean mantle. J. Geophys. Res. 108. doi:10.1029/2001JB001690

Famin, V., Nakashima, S., 2005. Hydrothermal fluid venting along a seismogenic detachment fault in the Moresby Rift (Woodlark Basin, Papua New Guinea). Geochem. Geophys. Geosystems - G Super 3 6. doi:10.1029/2005GC001112

Famin, V., Nakashima, S., Jolivet, L., Philippot, P., 2004. Mobility of metamorphic fluids inferred from infrared microspectroscopy on natural fluid inclusions: the example of Tinos Island, Greece. Contrib. Mineral. Petrol. 146, 736–749. doi:10.1007/s00410-003-0531-5

Famin, V., Philippot, P., Jolivet, L., Agard, P., 2004. Evolution of hydrothermal regime along a crustal shear zone, Tinos Island, Greece. Tectonics 23, n/a–n/a. doi:10.1029/2003TC001509

Faure, M., Bonneau, M., Pons, J., 1991. Ductile deformation and syntectonic granite emplacement during the late Miocene extension of the Aegea (Greece). Bull. Soc. Geol. Fr. 162, 3–11.

Fischer, G.J., Paterson, M.S., 1989. Dilatancy during rock deformation at high temperatures and pressures. J. Geophys. Res. Solid Earth 94, 17607–17617. doi:10.1029/JB094iB12p17607

Frenzel, M., Woodcock, N.H., 2014. Cockade breccia: Product of mineralisation along dilational faults. J. Struct. Geol. 68, 194–206. doi:10.1016/j.jsg.2014.09.001

Fricke, H., Wickham, S., O'Neil, J., 1992. Oxygen and hydrogen isotope evidence for meteoric water infiltration during mylonitization and uplift in the Ruby Mountains-East Humboldt Range core complex, Nevada. Contrib. Mineral. Petrol. 111, 203.

Fulignati, P., Kamenetsky, V.S., Marianelli, P., Sbrana, A., Mernagh, T.P., 2001. Melt inclusion record of immiscibility between silicate, hydrosaline, and carbonate melts; applications to skarn genesis at Mount Vesuvius. Geol. Boulder 29, 1043–1046.

Gautier, P., Brun, J.-P., 1994. Ductile crust exhumation and extensional detachments in the central Aegean (Cyclades and Evvia Islands). Geodin. Acta 7, 57–85. doi:10.1080/09853111.1994.11105259

Grasemann B, Zamolyi A, Petrakakis K, Rambousek C, Igelseder C (2002) Ein neuer metamorphic core complex in den West- Kykladen (Serifos, Greichenland). Erlanger Geologische Abh 3:36–37

Grasemann, B., Petrakakis, K., 2007. Evolution of the Serifos metamorphic core complex. J. Virtual Explor. 27, 1–18.

Grasemann, B., Schneider, D.A., Stockli, D.F., Iglseder, C., 2012. Miocene bivergent crustal extension in the Aegean: Evidence from the western Cyclades (Greece). Lithosphere 4, 23–39. doi:10.1130/L164.1

Griggs, D., 1974. A Model of Hydrolytic Weakening in Quartz. J. Geophys. Res. 79, 1653–1661. doi:10.1029/JB079i011p01653

Gueydan, F., Leroy, Y.M., Jolivet, L., Agard, P., 2003. Analysis of continental midcrustal strain localization induced by microfracturing and reaction-softening. J. Geophys. Res. 108. doi:10.1029/2001JB000611

Guillaume, B., Husson, L., Funiciello, F., Faccenna, C., 2013. The dynamics of laterally variable subductions; laboratory models applied to the Hellenides. Solid Earth SE Gottingen 4, 179–200.

Healy, D., 2009. Anisotropy, pore fluid pressure and low angle normal faults. J. Struct. Geol. 31, 561–574. doi:10.1016/j.jsg.2009.03.001

Hejl, E., Riedl, H., Weingartner, H., 2002. Post-plutonic unroofing and morphogenesis of the Attic–Cycladic complex (Aegea, Greece). Tectonophysics 349, 37–56. doi:10.1016/S0040-1951(02)00045-8

Holk, G.J., Taylor Jr., H.P., 2007. 18O/16O Evidence for Contrasting Hydrothermal Regimes Involving Magmatic and Meteoric-Hydrothermal Waters at the Valhalla Metamorphic Core Complex, British Columbia. Econ. Geol. Bull. Soc. Econ. Geol. 102, 1063.

Huet, B., Jolivet, L. (Directeur de thèse / A. (for a thesis or dissertation)), 2010. Rhéologie de la lithosphère continentale (l exemple de la mer Egée) (French). Université Pierre et Marie Curie.

Iacono-Marziano, G., Gaillard, F., Pichavant, M., 2008. Limestone assimilation by basaltic magmas; an experimental re-assessment and application to Italian volcanoes. Contrib. Mineral. Petrol. 155, 719–738. doi:10.1007/s00410-007-0267-8

Iacono Marziano, G., Gaillard, F., Pichavant, M., 2007. Limestone assimilation and the origin of CO2 emissions at the Alban Hills (Central Italy): Constraints from experimental petrology. J. Volcanol. Geotherm. Res. 166, 91–105. doi:10.1016/j.jvolgeores.2007.07.001

Iacono-Marziano, G., Gaillard, F., Scaillet, B., Pichavant, M., Chiodini, G., 2009. Role of non-mantle CO2 in the dynamics of volcano degassing: The Mount Vesuvius example. Geology 37, 319–322. doi:10.1130/G25446A.1

Iglseder, C., Grasemann, B., Rice, A.H.N., Petrakakis, K., Schneider, D.A., 2011. Miocene south directed low-angle normal fault evolution on Kea Island (West Cycladic Detachment System, Greece). Tectonics 30, n/a–n/a. doi:10.1029/2010TC002802

Iglseder, C., Grasemann, B., Schneider, D.A., Petrakakis, K., Miller, C., Klötzli, U.S., Thöni, M., Zámolyi, A., Rambousek, C., 2009. I and S-type plutonism on Serifos (W-Cyclades, Greece). Tectonophysics 473, 69–83. doi:10.1016/j.tecto.2008.09.021

Iglseder, C., Grasemann, B., Schneider, D., Rice, A.H.N., Lenauer, I., Mueller, M., Moertl, G., Voit, K., Petrakakis, K., Draganits, E., 2008. Low-angle normal fault mechanics and architecture in the Western Cyclades (Greece). Geophys. Res. Abstr. 10, @EGU2008–a–07793.

Jansen, J.B.H., Kraats, A.H., Rijst, H., Schulung, R.D., 1978. Metamorphism of siliceous dolomites at Naxos, Greece. Contrib. Mineral. Petrol. 67, 279–288. doi:10.1007/BF00381455

Jolivet, L., Augier, R., Faccenna, C., Negro, F., Rimmele, G., Agard, P., Robin, C., Rossetti, F., Crespo-Blanc, A., 2008. Subduction, convergence and the mode of backarc extension in the Mediterranean region. Bull. Soc. Geol. Fr. 179, 525–550. doi:10.2113/gssgfbull.179.6.525

Jolivet, L., Brun, J.-P., Gautier, P., Lallemant, S., Patriat, M., 1994. 3D-kinematics of extension in the Aegean region from the early Miocene to the present; insights from the ductile crust. Bull. Société Géologique Fr. 165, 195–209.

Jolivet, L., Brun, J.-P., 2010. Cenozoic geodynamic evolution of the Aegean. Int. J. Earth Sci. 99, 109–138. doi:10.1007/s00531-008-0366-4

Jolivet, L., Faccenna, C., 2000. Mediterranean extension and the Africa-Eurasia collision. Tectonics 19, 1095–1106. doi:10.1029/2000TC900018

Jolivet, L., Famin, V., Mehl, C., Parra, T., Aubourg, C., Hébert, R., Philippot, P., 2004. Strain localization during crustal-scale boudinage to form extensional metamorphic domes in the

Aegean Sea, in: Gneiss Domes in Orogeny. Geological Society of America, Boulder, Colorado, pp. 185–210.

Jolivet, L., Faccenna, C., Huet, B., Labrousse, L., Le Pourhiet, L., Lacombe, O., Lecomte, E., Burov, E., Denèle, Y., Brun, J.-P., Philippon, M., Paul, A., Salaün, G., Karabulut, H., Piromallo, C., Monié, P., Gueydan, F., Okay, A.I., Oberhänsli, R., Pourteau, A., Augier, R., Gadenne, L., Driussi, O., 2013. Aegean tectonics: Strain localisation, slab tearing and trench retreat. Tectonophysics 597-598, 1–33. doi:10.1016/j.tecto.2012.06.011

Jolivet, L., Lecomte, E., Huet, B., Denèle, Y., Lacombe, O., Labrousse, L., Le Pourhiet, L., Mehl, C., 2010. The North Cycladic Detachment System. Earth Planet. Sci. Lett. 289, 87–104. doi:10.1016/j.epsl.2009.10.032

Jolivet, L., Menant, A., Sternai, P., Rabillard, A., Arbaret, L., Augier, R., Laurent, V., Beaudoin, A., Grasemann, B., Huet, B., Labrousse, L., Le Pourhiet, L., 2015. The geological signature of a slab tear below the Aegean. Tectonophysics 659, 166–182. doi:10.1016/j.tecto.2015.08.004

Katzir, Y., Matthews, A.L.A.N., Garfunkel, Z., Schliestedt, M., Avigad, D., 1996. The tectono-metamorphic evolution of a dismembered ophiolite (Tinos, Cyclades, Greece). Geol. Mag. 133, 237–254.

Keay, S., Lister, G., Buick, I., 2001. The timing of partial melting, Barrovian metamorphism and granite intrusion in the Naxos metamorphic core complex, Cyclades, Aegean Sea, Greece. Tectonophysics 342, 275–312. doi:10.1016/S0040-1951(01)00168-8

Kerrich, R., Rehrig, W., 1987. Fluid motion associated with Tertiary mylonitization and detachment faulting: 18O/16O evidence from the Picacho metamorphic core complex, Arizona. Geology 15, 58–62.

Ktenas, C., 1917. Sur les relations pétrographiques, existant entre l'île de Serifos et les formations environnantes. Comptes Rendus Acad. Sci. v.158, 878.

Kumerics, C., Ring, U., Brichau, S., Glodny, J., Monie, P., 2005. The extensional Messaria shear zone and associated brittle detachment faults, Aegean Sea, Greece. J. Geol. Soc. 162, 701–721. doi:10.1144/0016-764904-041

Laurent, V., Beaudoin, A., Jolivet, L., Arbaret, L., Augier, R., Rabillard, A., Menant, A., 2015. Interrelations between extensional shear zones and synkinematic intrusions: The example of Ikaria Island (NE Cyclades, Greece). Tectonophysics. doi:10.1016/j.tecto.2015.03.020

Lecomte, E., Jolivet, L., Lacombe, O., Denèle, Y., Labrousse, L., Le Pourhiet, L., 2010. Geometry and kinematics of Mykonos detachment, Cyclades, Greece: Evidence for slip at shallow dip. Tectonics 29, n/a–n/a. doi:10.1029/2009TC002564

Leleu, M., Morikis, A., Picot, P., 1973. Sur des mineralisations de type skarn au Laurium (Grece). Miner. Skarn Type Laurion Greece 8, 259–263.

Le Pichon, X., Angelier, J., 1981. The Aegean Sea. Philos. Trans. R. Soc. Math. Phys. Eng. Sci. 300, 357–372.

Li, G., Sizaret, S., Branquet, Y., Barbanson, L., Chen, Y., Wang Bo, Wu Changzhi, Gu Lianxing, Shu Liangshu, 2014. Initial geometry and paleoflow reconstruction of the Yamansu skarn-related iron deposit of eastern Tian Shan (China) from paleomagnetic and magnetic fabrics investigations. J. Asian Earth Sci. 93, 1–14. doi:10.1016/j.jseaes.2014.06.009

Liati, A., Skarpelis, N., Pe-Piper, G., 2009. Late Miocene magmatic activity in the Attic-Cycladic Belt of the Aegean (Lavrion, SE Attica, Greece); implications for the geodynamic evolution and timing of ore deposition. Geol. Mag. 146, 732–742. doi:10.1017/S0016756809006438

Lister, G.S., Baldwin, S.L., 1993. Plutonism and the origin of metamorphic core complexes. Geology 21, 607. doi:10.1130/0091-7613(1993)021<0607:PATOOM>2.3.CO;2

Lister, G.S., Banga, G., Feenstra, A., 1984. Metamorphic core complexes of Cordilleran type in the Cyclades, Aegean Sea, Greece. Geology 12, 221. doi:10.1130/0091-7613(1984)12<221:MCCOCT>2.0.CO;2

Liu, J., Walter, J.M., Weber, K., 2002. Fluid-enhanced low-temperature plasticity of calcite marble: Microstructures and mechanisms. Geology 30, 787.

Logan, J.M., Hastedt, M., Lehnert, D., Denton, M., 1993. A case study of the properties of marble as building veneer. Int. J. Rock Mech. Min. Sci. Geomech. Abstr. 30, 1531–1537.

Long, K.R., 1992. Preliminary descriptive deposit model for detachment-fault-related mineralization (No. 8755531X). U. S. Geological Survey : Reston, VA, United States, United States.

Lorilleux, G., Cuney, M., Jébrak, M., Rippert, J. c., Portella, P., 2003. Chemical brecciation processes in the Sue unconformity-type uranium deposits, Eastern Athabasca Basin (Canada). J. Geochem. Explor. 80, 241. doi:10.1016/S0375-6742(03)00193-6

Lucas, I., 1999. Le pluton de Mykonos-Delos-Rhenee (Cyclades, Grèce): un exemple de mise en place synchrone de l'extension crustale (Ph.D thesis). Université d'Orléans, Orléans, France.

Maineri, C., Benvenuti, M., Costagliola, P., Dini, A., Lattanzi, P., Ruggieri, G., Villa, I.M., 2003. Sericitic alteration at the La Crocetta deposit (Elba Island, Italy): interplay between magmatism, tectonics and hydrothermal activity. Miner. Deposita 38, 67.

Malinverno, A., Ryan, W.B.F., 1986. Extension in the Tyrrhenian Sea and shortening in the Apennines as result of arc migration driven by sinking of the lithosphere. Tectonics 5, 227–245. doi:10.1029/TC005i002p00227

Maluski, H., Bonneau, M., Kienast, J.R., 1987. Dating the metamorphic events in the Cycladic area; 39 Ar/40 Ar data from metamorphic rocks of the Island of Syros (Greece). Bull. Société Géologique Fr. 3, 833–842.

Marchev, P., Kaiser-Rohrmeier, M., Heinrich, C., Ovtcharova, M., von Quadt, A., Raicheva, R., 2005. Hydrothermal ore deposits related to post-orogenic extensional magmatism and core complex formation; the Rhodope Massif of Bulgaria and Greece. Ore Geol. Rev. 27, 53–89. doi:10.1016/j.oregeorev.2005.07.027

Marinos, G., 1951. Geology and metallogeny of Serifos island. Geol. Geophys. Res. 1, 95–127.

Marinos, G. and Petrascheck, W.E., 1956. Larium: Geological and geophysical research. Inst. Geol. Subsurface Res., 4, 246.

McClusky, S., Balassanian, S., Barka, A., Demir, C., Ergintav, S., Georgiev, I., Gurkan, O., Hamburger, M., Hurst, K., Kahle, H., Kastens, K., Kekelidze, G., King, R., Kotzev, V., Lenk, O., Mahmoud, S., Mishin, A., Nadariya, M., Ouzounis, A., Paradissis, D., Peter, Y., Prilepin, M., Reilinger, R., Sanli, I., Seeger, H., Tealeb, A., Toksöz, M.N., Veis, G., 2000. Global Positioning System constraints on plate kinematics and dynamics in the eastern Mediterranean and Caucasus. J. Geophys. Res. 105, 5695. doi:10.1029/1999JB900351

Meinert, L.D., 1992. Skarns and Skarn Deposits. Geosci. Can. 19.

Meinert, L., Dipple, G., Nicolescu, S., 2005. World skarn deposits in Hedenquist, J.W., et al., eds., Economic Geology 100th Anniversary Volume: Littleton, Colorado, Society of Economic Geologists, p. 299–336.

Menand, T., 2008. The mechanics and dynamics of sills in layered elastic rocks and their implications for the growth of laccoliths and other igneous complexes. Earth Planet. Sci. Lett. 267, 93–99. doi:10.1016/j.epsl.2007.11.043

Menant, A., Jolivet, L., Augier, R., Skarpelis, N., 2013. The North Cycladic Detachment System and associated mineralization, Mykonos, Greece: Insights on the evolution of the Aegean domain. Tectonics 32, 433–452. doi:10.1002/tect.20037

Michel, J., Baumgartner, L., Putlitz, B., Schaltegger, U., Ovtcharova, M., 2008. Incremental growth of the Patagonian Torres del Paine Laccolith over 90 k.y. Geol. Boulder 36, 459–462. doi:10.1130/G24546A.1

Morrison, J., Anderson, J. Lawford, 1998. Footwall refrigeration along a detachment fault: Implications for the thermal evolution of core complexes. Science 279, 63–66.

Mulch, A., Teyssier, C., Cosca, M.A., Vennemann, T.W., 2006. Thermomechanical analysis of strain localization in a ductile detachment zone. Tectonics 111, doi:10.1029/2005JB004032.

Myers, I.A., Smith, E.I., Wyman, R.V., 1986. Control of gold mineralization at the Cyclopic Mine, Gold Basin District, Mohave County, Arizona. Econ. Geol. Bull. Soc. Econ. Geol. 81, 1553–1557.

Pérouse, E., Chamot-Rooke, N., Rabaute, A., Briole, P., Jouanne, F., Georgiev, I., Dimitrov, D., 2012. Bridging onshore and offshore present-day kinematics of central and eastern Mediterranean: Implications for crustal dynamics and mantle flow: CENTRAL TO EAST MEDITERRANEAN KINEMATICS. Geochem. Geophys. Geosystems 13, n/a–n/a. doi:10.1029/2012GC004289

Petrakakis, K., Zámolyi, A., Iglseder, C., Rambousek, C., Grasemann, B., Draganits, E. & Photiadis, A. 2013. Serifos Island sheet. Geological map of Greece, 1:50,000, Institute of Geology and Mineral Exploration & Studies, Athens.

Pons, J.M., Franchini, M., Meinert, L., Recio, C., Etcheverry, R., 2009. Iron skarns of the Vegas Peladas District, Mendoza, Argentina. Econ. Geol. Bull. Soc. Econ. Geol. 104, 157–184. doi:10.2113/gsecongeo.104.2.157

Rabillard, A., Arbaret, L., Jolivet, L., Le Breton, N., Gumiaux, C., Augier, R., Grasemann, B., 2015. Interactions between plutonism and detachments during metamorphic core complex formation, Serifos Island (Cyclades, Greece). Tectonics 34, 1080–1106. doi:10.1002/2014TC003650

Reynolds, S.J., Lister, G.S., 1987. Structural aspects of fluid-rock interactions in detachment zones. Geol. Boulder 15, 362–366.

Ring, U., Glodny, J., Will, T.M., Thomson, S., 2011. Normal faulting on Sifnos and the South Cycladic Detachment System, Aegean Sea, Greece. J. Geol. Soc. 168, 751–768. doi:10.1144/0016-76492010-064

Ring, U., Glodny, J., Will, T., Thomson, S., 2010. The Hellenic Subduction System: High-Pressure Metamorphism, Exhumation, Normal Faulting, and Large-Scale Extension. Annu. Rev. Earth Planet. Sci. 38, 45–76. doi:10.1146/annurev.earth.050708.170910

Roche, V., Laurent, V., Cardello, G.L., Jolivet, L., Scaillet, S., 2016. Anatomy of the Cycladic Blueschist Unit on Sifnos Island (Cyclades, Greece). J. Geodyn. doi:10.1016/j.jog.2016.03.008

Roman-Berdiel, T., Gapais, D., Brun, J.P., 1995. Analogue models of laccolith formation. J. Struct. Geol. 17, 1337–1346.

Rossetti, F., Tecce, F., Billi, A., Brilli, M., 2007. Patterns of fluid flow in the contact aureole of the Late Miocene Monte Capanne pluton (Elba Island, Italy): the role of structures and rheology. Contrib. Mineral. Petrol. 153, 743–760. doi:10.1007/s00410-006-0175-3

Royden, L.H., 1993. Evolution of retreating subduction boundaries formed during continental collision. Tectonics 12, 629–638. doi:10.1029/92TC02641

Royden, L.H., Papanikolaou, D.J., 2011. Slab segmentation and late Cenozoic disruption of the Hellenic arc. Geochem. Geophys. Geosystems 12, n/a–n/a. doi:10.1029/2010GC003280

Rutter, E.H., 1974. The influence of temperature, strain rate and interstitial water in the experimental deformation of calcite rocks. Tectonophysics 22, 311–334.

Salemink, J., 1985. Skarn and ore formation at Serifos, Greece, as a consequence of granodiorite intrusion. University of Utrecht, Utrecht.

Salemink, J., 1980. On the geology and petrology of Seriphos Island (Cyclades, Greece). Ann. Geol. Pays Hell. 30, 342–365.

Schenk, O., Urai, J.L., van der Zee, W., 2007. Evolution of boudins under progressively decreasing pore pressure; a case study of pegmatites enclosed in marble deforming at high grade metamorphic conditions, Naxos, Greece. Am. J. Sci. 307, 1009–1033. doi:10.2475/07.2007.03

Schneider, D.A., Senkowski, C., Vogel, H., Grasemann, B., Iglseder, C., Schmitt, A.K., 2011. Eocene tectonometamorphism on Serifos (western Cyclades) deduced from zircon depth-profiling geochronology and mica thermochronology. Lithos 125, 151–172. doi:10.1016/j.lithos.2011.02.005

Seidel, M., Pack, A., Sharp, Z.D., Seidel, E., 2005. The Kakopetros and Ravdoucha iron-oxide deposits, western Crete, Greece; fluid transport and mineralization within a detachment zone. Econ. Geol. Bull. Soc. Econ. Geol. 100, 165–174. doi:10.2113/100.1.0165

Sibson, R.H., 2000. Fluid involvement in normal faulting. J. Geodyn. 29, 469–499.

Sibson, R.H., 1986. Brecciation processes in fault zones; inferences from earthquake rupturing. Pure Appl. Geophys. 124, 159–175.

Sibson, R.H., 1985. A note on fault reactivation. J. Struct. Geol. 7, 751–754. doi:10.1016/0191-8141(85)90150-6

Skarpelis, N., 2002. Geodynamics and evolution of the Miocene mineralization in the Cycladic-Pelagonian belt, Hellenides. Bull Geol Soc Greece XXXIV(6), 2191–2206.

Skarpelis, N., 2007. The Lavrion deposit (SE Attica, Greece): geology, mineralogy and minor elements chemistry. Neues Jahrb. Für Mineral. - Abh. 183, 227–249. doi:10.1127/0077-7757/2007/0067

Skarpelis, N., Argyraki, A., 2009. Geology and origin of supergene Ore at the Lavrion Pb-Ag-Zn deposit, Attica, Greece. Resour. Geol. Tokyo 1998 59, 1–14. doi:10.1111/j.1751-3928.2008.00076.x

Skarpelis, N., Tsikouras, B., Pe-Piper, G., 2008. The Miocene igneous rocks in the Basal Unit of Lavrion (SE Attica, Greece); petrology and geodynamic implications. Geol. Mag. 145, 1–15. doi:10.1017/S0016756807003949

Smith, B.M., Reynolds, S.J., Day, H.W., Bodnar, R.J., 1991. Deep-seated fluid involvement in ductile-brittle deformation and mineralization, South Mountains metamorphic core complex, Arizona; with Suppl. Data 91-09. Geol. Soc. Am. Bull. 103, 559–569. doi:10.1130/0016-7606(1991)103<0559:DSFIID>2.3.CO;2

Smith, S.A.F., Holdsworth, R.E., Collettini, C., 2011. Interactions between low-angle normal faults and plutonism in the upper crust: Insights from the Island of Elba, Italy. Geol. Soc. Am. Bull. 123, 329–346. doi:10.1130/B30200.1

Spencer, J.E., Welty, J.W., 1986. Possible controls of base- and precious-metal mineralization associated with Tertiary detachment faults in the lower Colorado River trough, Arizona and California. Geol. Boulder 14, 195–198.

Spry, P., Mathur, R., Bonsall, T., Voudouris, P., Melfos, V., 2014. Re-Os isotope evidence for mixed source components in carbonate-replacement Pb-Zn-Ag deposits in the Lavrion district, Attica, Greece. Mineral. Petrol. 108, 503–513. doi:10.1007/s00710-013-0314-2

Stampfli, G.M., 2000. Tethyan oceans. Geol. Soc. Lond. Spec. Publ. 173, 1–23. doi:10.1144/GSL.SP.2000.173.01.01

Stouraiti, C., Mitropoulos, P., Tarney, J., Barreiro, B., McGrath, A.M., Baltatzis, E., 2010. Geochemistry and petrogenesis of late Miocene granitoids, Cyclades, southern Aegean: Nature of source components. Lithos 114, 337–352. doi:10.1016/j.lithos.2009.09.010

St. Seymour, K., Zouzias, D., Tombros, S., Kolaiti, E., 2009. Geochemistry of the Serifos pluton (Cycladic islands) and associated iron oxide and sulfide ores: Skarn or metamorphosed exhalite deposits? Neues Jahrb. Für Mineral. - Abh. 186, 249–270. doi:10.1127/0077-7757/2009/0143

Paterson, S.R., Tobisch, O.T., 1992. Rates of processes in magmatic arcs: implications for the timing and nature of pluton emplacement and wall rock deformation. J. Struct. Geol. 14,291–300.

Taylor, B.E., 1986. Magmatic volatiles; isotopic variation of C, H, and S. Rev. Mineral. Geochem. 16, 185–225.

Tschegg, C., Grasemann, B., 2009. Deformation and alteration of a granodiorite during low-angle normal faulting (Serifos, Greece). Lithosphere 1, 139–154. doi:10.1130/L33.1

Tullis, J., Yund, R. a., 1977. Experimental deformation of dry Westerly granite. J Geophys Res U. S. 5705.

Urai, J.L., Schuiling, R.D., Jansen, J.B.H., 1990. Alpine deformation on Naxos (Greece). Geol. Soc. Lond. Spec. Publ. 54, 509–522. doi:10.1144/GSL.SP.1990.054.01.47

Van Hinsbergen, D.J.J., Hafkenscheid, E., Spakman, W., Meulenkamp, J.E., Wortel, R., 2005. Nappe stacking resulting from subduction of oceanic and continental lithosphere below Greece. Geology 33, 325. doi:10.1130/G20878.1

Vergouwen, L., 1976. Skarnmineralisaties of Serifos. Intern Rep. Dept Geochem UnivUtrecht 90.

Verkaeren, J., 1971. Les grenats birefringents des skarns a magnetite de San Leone (Sardaigne SW). Birefringent Garnets San Leone Magn. Skarn Depos. Southwest. Sard. 94, 492–499.

Voudouris, P., Melfos, V., Spry, P.G., Bonsall, T., Tarkian, M., Economou-Eliopoulos, M., 2008. Mineralogical and fluid inclusion constraints on the evolution of the Plaka Intrusion-related ore system, Lavrion, Greece. Mineral. Petrol. 93, 79–110. doi:10.1007/s00710-007-0218-0

Wickham, S.M. (analytic), Peters, M.T. (analytic), Fricke, H.C. (analytic), O'neil, J.R. (analytic), 1993. Identification of magmatic and meteoric fluid sources and upward- and downward-moving infiltration fronts in a metamorphic core complex (English). Geol. Boulder 21, 81–84.

Wijbrans, J.R., McDougall, I., 1988. Metamorphic evolution of the Attic Cycladic Metamorphic Belt on Naxos (Cyclades, Greece) utilizing 40Ar/39Ar age spectrum measurements. J. Metamorph. Geol. 6, 571–594. doi:10.1111/j.1525-1314.1988.tb00441.x

Wortel, M.J.R., Spakman, W., 2000. Subduction and Slab Detachment in the Mediterranean-Carpathian Region. Science 1910.

Highlights

Exhaustive description of MT and HT Serifos skarns in relation with detachments

HT skarns are mainly endoskarn by replacing granodiorite and MT skarn are exoskarn

Fluids responsible of skarn formation mostly came from the granodiorite body

Syn-kinematic skarns show how intrusion-related fluids interfere with detachments

Skarns suffered ductile-brittle deformation along detachment during their emplacement

Detachments acting as crustal drains and magmatic fluid flows is not pluton-centred

Supplementary materails (SM)

SM1: Numerical 3D model of the Serifos lithostratigraphic unit.

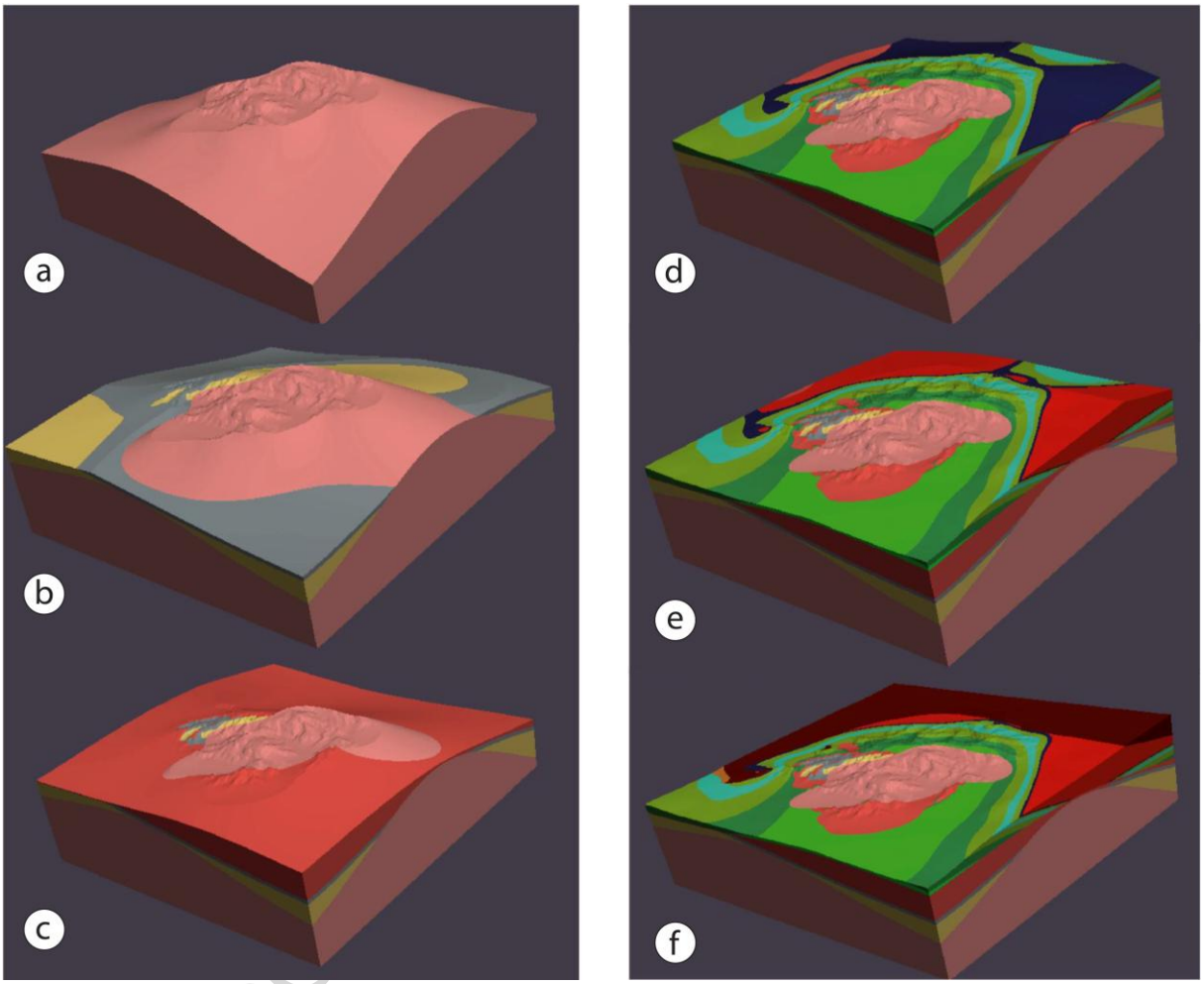

Result of 3D modelisation with "Geomodeller" software from the interpolation of geological contours. Progressive stacking of units order to obtain the final model of the island of Serifos.

a) *The granodiorite is the most recently established unit. With "Erode" function assigned to it under "Geomodeller", it cuts across the whole older metamorphic units. The depths structures not being constrained by structural data, so the extrapolating form is an artifact effect that is not to take into consideration*

b) *The Cycladic Continental Basement Unit composed by gneiss and marbles are the deepest units and therefore the first in the geological stack. It is intruded by the granodiorite.*

c) *The lower Meghàlo Livadhi detachment set up into mylonitic marbles and crosscut metamorphic structures within a narrow strip delimited by two formation (red level) in the geological stack of "Geomodeller"*

d) *Green-schists and amphibolites are represented by three formations for each unit to observe internal deformation in the Cycladic Blueschist Unit. Ultramylonitic marbles are localised on top of the CBU.*

e) *This ultramylonitic marble was affected by deformation of the second detachment (Kávos Kiklopas detachment: bright red level) that too crosscut the older metamorphic units. By extrapolation the detachment plane is not cross by the granodiorite intrusion.*

f) *The ankiritised schists and metaophiolites of the Upper Cycladic Unit is overlying the Kávos Kiklopas detachment in "Geomodeller".*

SM2: Isotopic oxygen composition of Serifos skarns and mineralization compiled from Salemink (1985).

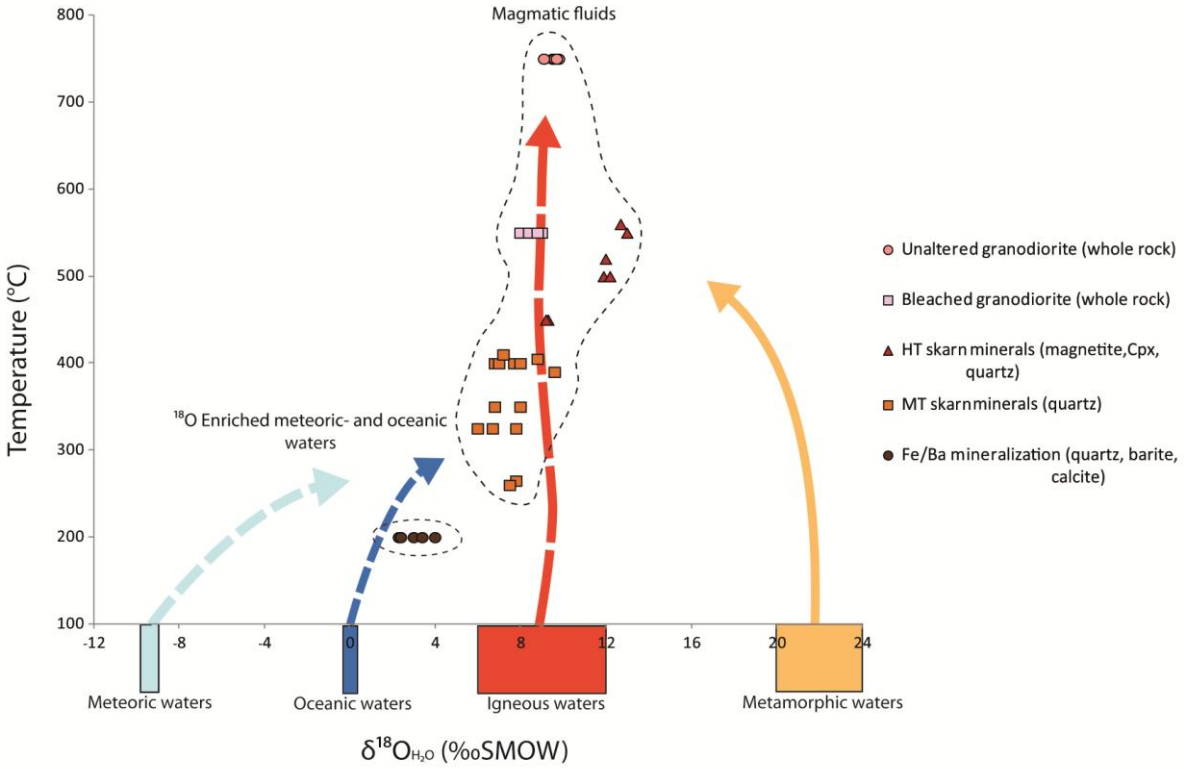

Salemink (1985) measured $\delta^{18}O_{H2O}$ values for unaltered and bleached granodiorite, as well as HT and MT skarns and Fe/Ba mineralization. We recompiled $\delta^{18}O$ data and plot it versus temperatures estimates derived from rough estimation for granodiorite crystallization (750°C) and from fluid inclusion homogenization temperature for skarns and mineralization. MT skarns present a slight negative shift of $\delta^{18}O_{H2O}$ values. In fact, available isotopic data do not document the evolution from prograde to retrograde stages of each type of skarns. Indeed, most of the data are issued from measurements on quartz that grow lately in the paragenetic evolution. Thus, the slight negative shift of $\delta^{18}O_{H2O}$ values mentioned above for MT skarns may be due to local opening and limited flow of external fluids during the retrograde stage. However, relative to negative $\delta^{18}O_{H2O}$ values obtained from retrogressive mineral phase on other skarns systems (e.g. Pons et al., 2009), no major contribution of oceanic/meteoric waters is recorded during the Serifos MT skarns genesis. Isotopic signature reservoir boxes are from Taylor (1986).

SM3: Mineralogy and petrography of the Garnet-Pyroxene endoskarns in marbles of CCBU at Vaghia location

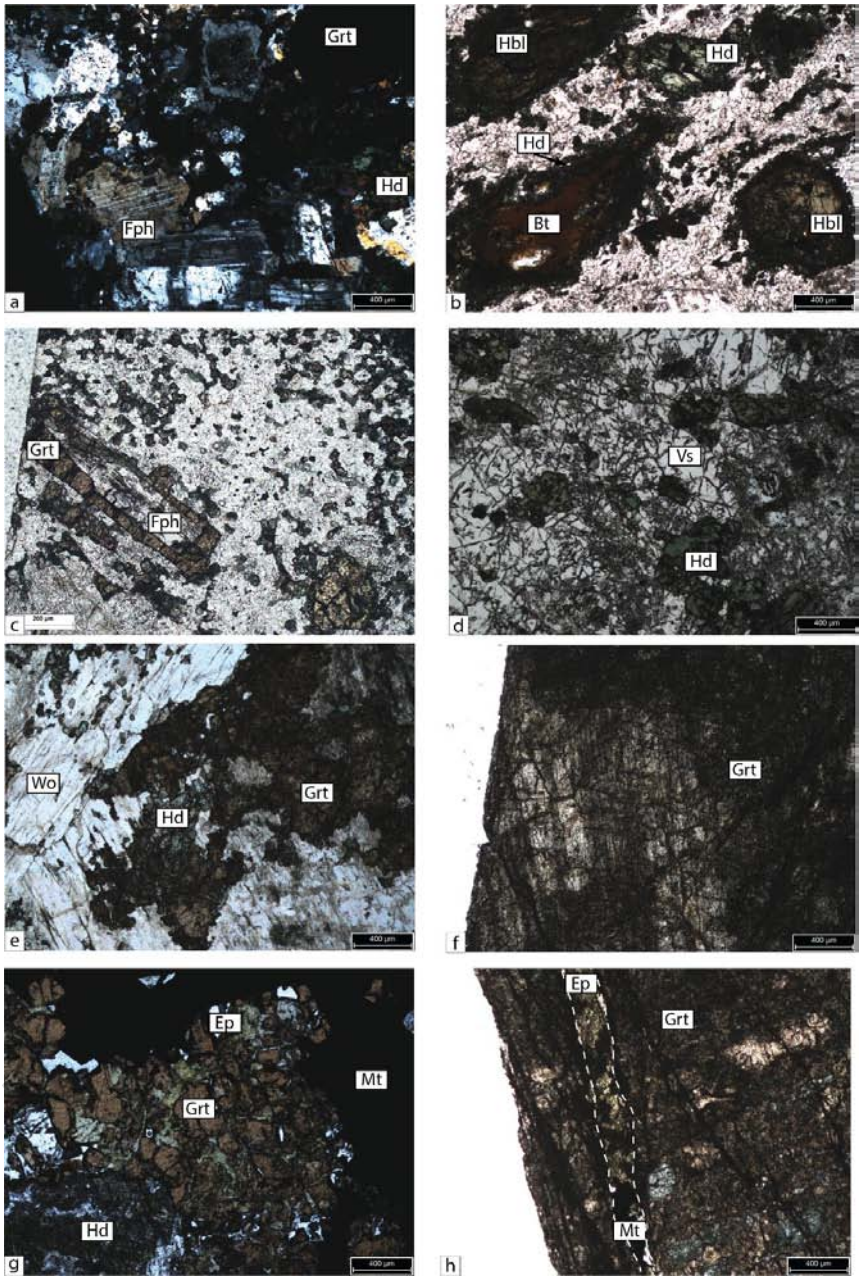

In "bubble" endoskarn facies, (a): primary magmatic microstructure replaced by andradite-hedenbergite assemblage; (b): biotite and hornblende with thin replacement rims of hedenbergite; (c): primary magmatic plagioclase feldspar with replacement rim of garnet; (d): vesuvianite in analyzed and polarized light; (e): wollastonite associated with andradite and hedenbergite; In "ribbon" endoskarn facies, (f): relict of magmatic microstructure (plagioclase laths) in anhedral garnet; (g): retrograde phase of ribbon endoskarn where garnet is pervasively replaced by magnetite and epidote; (h): epidote- and magnetite vein crosscutting garnet within endoskarn.

SM4: Mineralogy and petrography of the pyroxene +/- ilvaite skarn breccia regional level at the Meghàlo Livadhi bay location.

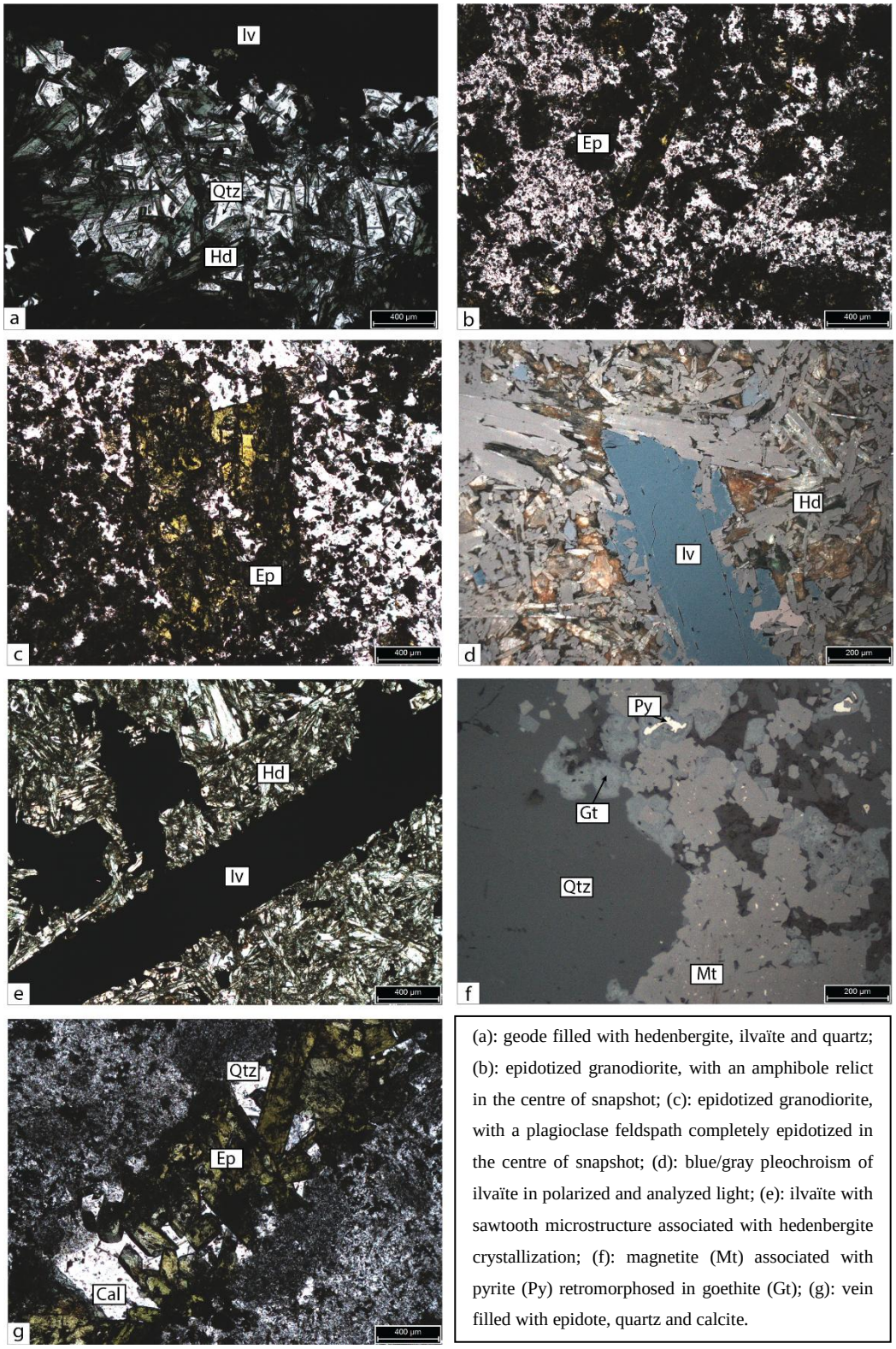

(a): geode filled with hedenbergite, ilvaïte and quartz; (b): epidotized granodiorite, with an amphibole relict in the centre of snapshot; (c): epidotized granodiorite, with a plagioclase feldspath completely epidotized in the centre of snapshot; (d): blue/gray pleochroism of ilvaïte in polarized and analyzed light; (e): ilvaïte with sawtooth microstructure associated with hedenbergite crystallization; (f): magnetite (Mt) associated with pyrite (Py) retromorphosed in goethite (Gt); (g): vein filled with epidote, quartz and calcite.

SM5: Mineralogy and petrography of the Kávos Kiklopas exoskarns skarns

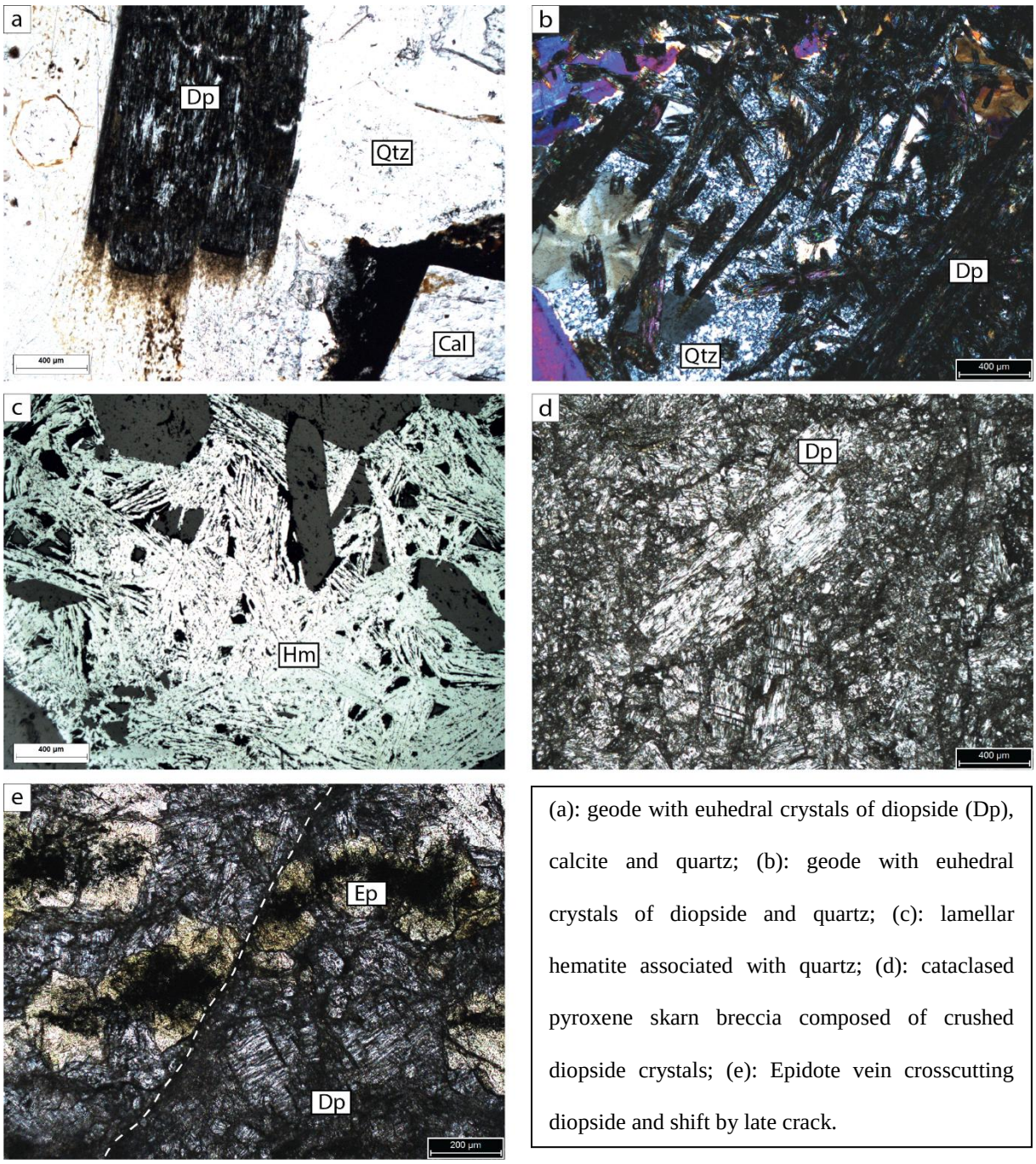

(a): geode with euhedral crystals of diopside (Dp), calcite and quartz; (b): geode with euhedral crystals of diopside and quartz; (c): lamellar hematite associated with quartz; (d): cataclased pyroxene skarn breccia composed of crushed diopside crystals; (e): Epidote vein crosscutting diopside and shift by late crack.

Highlights

- Exhaustive description of MT and HT Serifos skarns in relation with detachments
- HT skarns are mainly endoskarn by replacing granodiorite and MT skarn are exoskarn
- Fluids responsible of skarn formation mostly came from the granodiorite body
- Syn-kinematic skarns show how intrusion-related fluids interfere with detachments
- Skarns suffered ductile-brittle deformation along detachment during their emplacement
- Detachments acting as crustal drains and magmatic fluid flows is not pluton-centred